

Structure of Nondiffracting Waves and Some Interesting Applications

MICHEL ZAMBONI-RACHED

Centro de Ciências Naturais e Humanas, Universidade Federal do ABC,
Santo Andre, SP, Brazil

ERASMO RECAMI

Università degli Studi di Bergamo, Bergamo, Italy, and
INFN-Sezione di Milano, Milan, Italy

HUGO E. HERNÁNDEZ-FIGUEROA

Universidade Estadual de Campinas, Campinas, SP, Brazil

2.1 INTRODUCTION

Since early work [1–4] on *nondiffracting waves* (also called *localized waves*), a great deal has been published on this important subject from either the theoretical or experimental point of view. Initially, the theory was developed taking into account only free space; however, in recent years it has been extended to deal with more complex media, exhibiting effects such as dispersion [5–7], nonlinearity [8], anisotropy [9], and losses [10]. Such extensions have been carried out along with the development of efficient methods for obtaining nondiffracting beams and pulses in the subluminal, luminal, and superluminal regimes [11–18].

In this chapter we address some theoretical methods related to nondiffracting solutions of linear wave equations in unbounded homogeneous media and to interesting

applications of these waves. The usual cylindrical coordinates (ρ, ϕ, z) are used here. In these coordinates the linear wave equation is written as

$$\frac{1}{\rho} \frac{\partial}{\partial \rho} \left(\rho \frac{\partial \Psi}{\partial \rho} \right) + \frac{1}{\rho^2} \frac{\partial^2 \Psi}{\partial \phi^2} + \frac{\partial^2 \Psi}{\partial z^2} - \frac{1}{c^2} \frac{\partial^2 \Psi}{\partial t^2} = 0. \quad (2.1)$$

In Section 2.2 we analyze the general structure of localized waves, develop generalized bidirectional decomposition, and use it to obtain several luminal and superluminal nondiffracting wave solutions of Eq. (2.1). In Section 2.3 we develop a space–time focusing method through a continuous superposition of X-shaped pulses of different velocities. In Section 2.4 we address the properties of chirped optical X-shaped pulses propagating in material media without boundaries. Finally, in Section 2.5 we show how a suitable superposition of Bessel beams can be used to obtain stationary localized wave fields with high transverse localization whose longitudinal intensity pattern can assume any shape desired within a chosen interval $0 \leq z \leq L$ of the propagation axis.

Important Observation We call the reader’s attention to the fact that the sections in this chapter are essentially independent, and due to this fact, the notation is sometimes not standardized. For example, in Section 2.2 the longitudinal wave number is represented by k_z and one of the spectra parameters of the generalized bidirectional decomposition is denoted by β , whereas in Sections 2.4 and 2.5, β represents the longitudinal wave number.

2.2 SPECTRAL STRUCTURE OF LOCALIZED WAVES

An effective way to understand the concept of (ideal) nondiffracting waves is through a precise mathematical definition of these solutions so that we can extract from them the necessary spectral structure. Intuitively, an *ideal nondiffracting wave* (beam or pulse) can be defined as a wave capable of maintaining its spatial form (except for local variations) indefinitely while propagating. We can express this intuitive property by saying that a localized wave has to possess the property [12,13]

$$\Psi(\rho, \phi, z, t) = \Psi \left(\rho, \phi, z + \Delta z_0, t + \frac{\Delta z_0}{V} \right), \quad (2.2)$$

where Δz_0 is a certain length and V is the pulse propagation speed, which can assume any value here: $0 \leq V \leq \infty$. Using a Fourier–Bessel expansion, we can express a function $\Psi(\rho, \phi, z, t)$ as

$$\begin{aligned} & \Psi(\rho, \phi, z, t) \\ &= \sum_{n=-\infty}^{\infty} \left[\int_0^{\infty} dk_{\rho} \int_{-\infty}^{\infty} dk_z \int_{-\infty}^{\infty} d\omega k_{\rho} A'_n(k_{\rho}, k_z, \omega) J_n(k_{\rho} \rho) e^{ik_z z} e^{-i\omega t} e^{in\phi} \right]. \end{aligned} \quad (2.3)$$

Using the translation property of the Fourier transforms $T[f(x + a)] = \exp(ika)T[f(x)]$, we have that $A'_n(k_\rho, k_z, \omega)$ and $\exp[i(k_z \Delta z_0 - \omega \Delta z_0/V)] \times A'_n(k_\rho, k_z, \omega)$ are the Fourier–Bessel transforms of the left- and right-hand-side functions in Eq. (2.2). From this same equation we can get [12,13] the fundamental constraint linking the angular frequency ω and the longitudinal wave number k_z :

$$\omega = Vk_z + 2m\pi \frac{V}{\Delta z_0} \quad (2.4)$$

with m an integer. Obviously, this constraint can be satisfied through the spectral functions $A'_n(k_\rho, k_z, \omega)$.

Now let us mention explicitly that constraint (2.4) does not imply any breakdown of the wave equation validity. In fact, when inserting expression (2.3) in wave equation (2.2), we find that

$$\frac{\omega^2}{c^2} = k_z^2 + k_\rho^2. \quad (2.5)$$

So, to obtain a solution of the wave equation from (2.3), the spectrum $A'_n(k_\rho, k_z, \omega)$ must have the form

$$A'_n(k_\rho, k_z, \omega) = A_n(k_z, \omega) \delta \left(k_\rho^2 - \left(\frac{\omega^2}{c^2} - k_z^2 \right) \right), \quad (2.6)$$

where $\delta(\cdot)$ is the Dirac delta function. With this we can write a solution of the wave equation as

$$\begin{aligned} \Psi(\rho, \phi, z, t) &= \sum_{n=-\infty}^{\infty} \left[\int_0^{\infty} d\omega \int_{-\omega/c}^{\omega/c} dk_z A_n(k_z, \omega) J_n \left(\rho \sqrt{\frac{\omega^2}{c^2} - k_z^2} \right) e^{ik_z z} e^{-i\omega t} e^{in\phi} \right], \end{aligned} \quad (2.7)$$

where we have considered positive angular frequencies only. Equation (2.7) is a superposition of Bessel beams and it is understood that the integrations in the $\omega - k_z$ plane are confined to the region $0 \leq \omega \leq \infty$; $-\omega/c \leq k_z \leq \omega/c$.

To obtain an ideal nondiffracting wave, the spectra $A_n(k_z, \omega)$ must obey the fundamental constraint (2.4), so we write

$$A_n(k_z, \omega) = \sum_{m=-\infty}^{\infty} S_{nm}(\omega) \delta(\omega - (Vk_z + b_m)), \quad (2.8)$$

where the b_m are constants representing the terms $2m\pi V/\Delta z_0$ in Eq. (2.4) and the $S_{nm}(\omega)$ are arbitrary frequency spectra. With (2.8) in (2.7) we get a general integral

form of an ideal nondiffracting wave defined by Eq. (2.2):

$$\Psi(\rho, \phi, z, t) = \sum_{n=-\infty}^{\infty} \sum_{m=-\infty}^{\infty} \psi_{nm}(\rho, \phi, z, t), \quad (2.9)$$

with

$$\begin{aligned} \psi_{nm}(\rho, \phi, z, t) = & e^{-ib_m z/V} \int_{(\omega_{\min})_m}^{(\omega_{\max})_m} d\omega S_{nm}(\omega) \\ & \times J_n \left(\rho \sqrt{\left(\frac{1}{c^2} - \frac{1}{V^2} \right) \omega^2 + \frac{2b}{V^2} \omega - \frac{b^2}{V^2}} \right) e^{i(\omega/V)(z-Vt)} e^{in\phi}, \end{aligned} \quad (2.10)$$

where ω_{\min} and ω_{\max} depend on the values of V :

- For subluminal ($V < c$) localized waves: $b_m > 0$, $(\omega_{\min})_m = cb_m/(c + V)$ and $(\omega_{\max})_m = cb_m/(c - V)$.
- For luminal ($V = c$) localized waves: $b_m > 0$, $(\omega_{\min})_m = b_m/2$, and $(\omega_{\max})_m = \infty$.
- For superluminal ($V > c$) localized waves: $b_m \geq 0$, $(\omega_{\min})_m = cb_m/(c + V)$, and $(\omega_{\max})_m = \infty$; or $b_m < 0$, $(\omega_{\min})_m = cb_m/(c - V)$, and $(\omega_{\max})_m = \infty$.

It is important to notice that each $\psi_{nm}(\rho, \phi, z, t)$ in the superposition (2.9) is a truly nondiffracting wave (beam or pulse) and their superposition (2.9) is just the most general form available to represent a nondiffracting wave defined by Eq. (2.2). Due to this fact, the search for methods capable of providing analytical solutions for $\psi_{nm}(\rho, \phi, z, t)$, Eq. (2.10), becomes an important task.

Keep in mind that Eq. (2.10) is also a Bessel beam superposition but with the constraint (2.4) between their angular frequencies and longitudinal wave numbers. Despite the fact that expression (2.10) represents ideal nondiffracting waves, it is difficult to use it to obtain closed analytical solutions. Because of this, we are going to develop a method able to overcome this limitation, providing several interesting localized wave solutions (luminal and superluminal) in arbitrary frequencies, including some exhibiting finite energy.

2.2.1 Generalized Bidirectional Decomposition

For reasons that will soon become clear, instead of dealing with the integral expression (2.9), our starting point is the general expression (2.7). Here, for simplicity, we restrict ourselves to axially symmetric solutions assuming the spectral functions as

$$A_n(k_z, \omega) = \delta_{n0} A(k_z, \omega), \quad (2.11)$$

where δ_{n0} is the Kronecker delta. In this way, we get the following general solution (considering positive angular frequencies only) describing axially symmetric waves:

$$\Psi(\rho, \phi, z, t) = \int_0^\infty d\omega \int_{-\omega/c}^{\omega/c} dk_z A(k_z, \omega) J_0 \left(\rho \sqrt{\frac{\omega^2}{c^2} - k_z^2} \right) e^{ik_z z} e^{-i\omega t}. \quad (2.12)$$

As we have seen, ideal nondiffracting waves can be obtained since the spectrum $A(k_z, \omega)$ satisfies the linear relationship (2.4). In this way, it is natural to adopt new spectral parameters in place of (ω, k_z) that make it easier to implement that constraint [12,13].

With this in mind, we choose the new spectral parameters (α, β) through

$$\alpha = \frac{1}{2V}(\omega + V k_z), \quad \beta = \frac{1}{2V}(\omega - V k_z). \quad (2.13)$$

Let us consider here only luminal ($V = c$) and superluminal ($V > c$) nondiffracting pulses.

With the change of variables (2.13) in the integral solution (2.12), and considering $V \geq c$, the integration limits on α and β have to satisfy the three inequalities:

$$\begin{cases} 0 < \alpha + \beta < \infty \\ \alpha \geq \frac{c - V}{c + V} \beta \\ \alpha \geq \frac{c + V}{c - V} \beta. \end{cases} \quad (2.14)$$

Let us suppose both α and β to be positive [$\alpha, \beta \geq 0$]. The first inequality in (2.14) is then satisfied, whereas the coefficients $(c - V)/(c + V)$ and $(c + V)/(c - V)$ entering relations (2.14) are both negative (since $V > c$). As a consequence, the other two inequalities in (2.14) are satisfied automatically. In other words, the integration limits in $0 \leq \alpha \leq \infty$ and $0 \leq \beta \leq \infty$ are *contained* in the limits (2.14) and are therefore acceptable. Indeed, they constitute a rather suitable choice for facilitating all subsequent integrations.

Therefore, instead of Eq. (2.12) we consider the (more easily integrable) Bessel beam superposition in the new variables (with $V \geq c$)

$$\begin{aligned} \Psi(\rho, \zeta, \eta) = & \int_0^\infty d\alpha \int_0^\infty d\beta A(\alpha, \beta) \\ & \times J_0 \left(\rho \sqrt{\left(\frac{V^2}{c^2} - 1 \right) (\alpha^2 + \beta^2) + 2 \left(\frac{V^2}{c^2} + 1 \right) \alpha \beta} \right) e^{i\alpha \zeta} e^{-i\beta \eta}, \end{aligned} \quad (2.15)$$

where we have defined

$$\zeta \equiv z - Vt, \quad \eta \equiv z + Vt. \quad (2.16)$$

The present procedure is a generalization of the bidirectional decomposition technique, which was described earlier [11] for $V = c$.

From the new spectral parameters defined in transformation (2.13), it is easy to see that constraint (2.4) (i.e., $\omega = Vk_z + b$) is implemented just by making

$$A(k_z, \omega) \rightarrow A(\alpha, \beta) = S(\alpha)\delta(\beta - \beta_0), \quad (2.17)$$

with $\beta_0 = b/2V$. The delta function $\delta(\beta - \beta_0)$ in the spectrum (2.17) means that we are integrating Bessel beams along the continuous line $\omega = Vk_z + 2V\beta_0$, and in this way the function $S(\alpha)$ will give the frequency dependence of the spectrum: $S(\alpha) \rightarrow S(\omega/V - \beta_0)$. This method is a natural way of obtaining pulses with field concentration on $\rho = 0$ and $\zeta = 0 \rightarrow z = Vt$.

It is important to stress [13] that when $\beta_0 > 0$ in (2.17), the superposition (2.15) has contributions of both backward and forward Bessel beams in the frequency intervals $V\beta_0 \leq \omega < 2V\beta_0$ (where $k_z < 0$) and $2V\beta_0 \leq \omega \leq \infty$ (where $k_z \geq 0$), respectively. Nevertheless, we can obtain physical solutions when making the contribution of the backward components negligible by choosing suitable weight functions $S(\alpha)$. It is also important to note that we use the new spectral parameters α and β just to obtain (closed) analytical localized wave solutions, as the spectral characteristics of these new solutions can be brought into evidence just by using transformations (2.13) and writing the correspondent spectrum in terms of the usual ω and k_z spectral parameters.

In the following, we consider some cases with $\beta_0 = 0$ and $\beta_0 > 0$.

Closed Analytical Expressions Describing Some Ideal Nondiffracting Pulses Let us first consider, in Eq. (2.15), the following spectra of the type (2.17) with $\beta_0 = 0$:

$$A(\alpha, \beta) = \begin{cases} aV\delta(\beta)e^{-aV\alpha} & (2.18) \\ aV\delta(\beta)J_0(2d\sqrt{\alpha})e^{-aV\alpha} & (2.19) \\ \delta(\beta)\frac{\sin d\alpha}{\alpha}e^{-aV\alpha}, & (2.20) \end{cases}$$

with $a > 0$ and d being constants. One can obtain from these spectra the following superluminal localized wave solutions. From spectrum (2.18), we can use the identity (6.611.1) in [19] to obtain the well-known ordinary X-wave solution (also called an X-shaped pulse)

$$\Psi(\rho, \zeta) \equiv X = \frac{aV}{\sqrt{(aV - i\zeta)^2 + [(V^2/c^2) - 1]\rho^2}}. \quad (2.21)$$

Using spectrum (2.19) and identity (6.644.4) of [19], we get

$$\Psi(\rho, \zeta) = X \cdot J_0 \left(\sqrt{\frac{V^2}{c^2} - 1} (aV)^{-2} d^2 X^2 \rho \right) \exp[-(aV - i\zeta)(aV)^{-2} d^2 X^2]. \quad (2.22)$$

The superluminal nondiffracting pulse

$$\Psi(\rho, \zeta) = \sin^{-1} \left[2 \frac{d}{aV} \left(\sqrt{X^{-2} + (d/aV)^2 + 2\rho d(aV)^{-2} \sqrt{V^2/c^2 - 1}} + \sqrt{X^{-2} + (d/aV)^2 - 2\rho d(aV)^{-2} \sqrt{V^2/c^2 - 1}} \right)^{-1} \right] \quad (2.23)$$

is obtained from spectrum (2.21) using identity (6.752.1) of [19] for $a > 0$ and $d > 0$.

From the previous discussion we know that any solution obtained from spectra of the type (2.17) with $\beta_0 = 0$ is free of noncausal (backward) components. In addition, when $\beta_0 = 0$, we can see that the pulsed solutions depend on z and t through $\zeta = z - Vt$ only, and so propagate rigidly (i.e., without distortion). Such pulses can be localized transversally only if $V > c$, because if $V = c$, the function Ψ has to obey the Laplace equation on transverse planes [12,13].

Many others superluminal localized waves can easily be constructed [13] from the solutions above just by taking the derivatives (of any order) with respect to ζ . It is also possible to show [13] that new solutions obtained in this way have their spectra shifted toward higher frequencies.

Now, let us consider, in Eq. (2.15), a spectrum of the type (2.17) with $\beta_0 > 0$:

$$A(\alpha, \beta) = aV \delta(\beta - \beta_0) e^{-aV\alpha}, \quad (2.24)$$

with a a positive constant. As we have seen, the presence of the delta function with the constant $\beta_0 > 0$ implies that we are integrating (summing) Bessel beams along the continuous line $\omega = Vk_z + 2V\beta_0$. The function $S(\alpha) = aV \exp(-aV\alpha)$ means that we are considering a frequency spectrum of the type $S(\omega) \propto \exp(-a\omega)$ and therefore with a bandwidth given by $\Delta\omega = 1/a$.

Since $\beta_0 > 0$, the interval $V\beta_0 \leq \omega < 2V\beta_0$ (or, equivalently in this case, $0 \leq \alpha < \beta_0$) corresponds to backward Bessel beams (i.e., negative values of k_z). However, we can get physical solutions when making the contribution of this frequency interval negligible. In this case, it can be done by making $a\beta_0V \ll 1$, so that the exponential decay of the spectrum S with respect to ω is very slow and the contribution of the interval $\omega \geq 2V\beta_0$ (where $k_z \geq 0$) overruns the $V\beta_0 \leq \omega < 2V\beta_0$ (where $k_z < 0$) contribution.

We note that once we ensure the causal behavior of the pulse by making $aV\beta_0 \ll 1$ in (2.24), we have that the $\Delta\alpha = 1/aV \gg \beta_0$, so we can simplify the argument of the Bessel function in the integrand of superposition (2.15) by neglecting the term $(V^2/c^2 - 1)\beta_0^2$. With this, the superposition (2.15), with the spectrum (2.24), can be

written as

$$\begin{aligned} \Psi(\rho, \zeta, \eta) &\approx aV e^{-i\beta_0\eta} \\ &\times \int_0^\infty d\alpha J_0\left(\rho\sqrt{\left(\frac{V^2}{c^2}-1\right)\alpha^2+2\left(\frac{V^2}{c^2}+1\right)\alpha\beta_0}\right) e^{i\alpha\zeta} e^{-aV\alpha}. \end{aligned} \quad (2.25)$$

We can now use identity (6.616.1) of [19] and obtain the new localized superluminal solution called the *superluminal focus wave mode* (SFWM) [13]:

$$\Psi_{\text{SFWM}}(\rho, \zeta, \eta) = e^{-i\beta_0\eta} X \exp\left[\frac{\beta_0(V^2+c^2)}{V^2-c^2}((aV-i\zeta)-aVX^{-1})\right], \quad (2.26)$$

where, as before, X is the ordinary X pulse (2.21). The center of the SFWM is localized on $\rho = 0$ and $\zeta = 0$ (i.e., in $z = Vt$). The intensity, $|\Psi|^2$, of this pulse propagates rigidly, as a function of ρ and ζ only. However, the complex function Ψ_{SFWM} (i.e., its real and imaginary parts) propagates just with local variations, recovering their entire three-dimensional form after each space and time interval given by $\Delta z_0 = \pi/\beta_0$ and $\Delta t_0 = \pi/\beta_0 V$.

The SFWM solution given above for $V \rightarrow c^+$ reduces to the well-known *focus wave mode* (FWM) solution [11] traveling with speed c :

$$\Psi_{\text{FWM}}(\rho, \zeta, \eta) = ac \frac{e^{-i\beta_0\eta}}{ac-i\zeta} \exp\left(-\frac{\beta_0\rho^2}{ac-i\zeta}\right). \quad (2.27)$$

Let us also emphasize that since $\beta_0 > 0$, the resulting spectrum (2.24) is comprised of angular frequencies $\omega \geq V\beta_0$. Thus, our new solution can be used to construct high-frequency pulses.

Finite-Energy Nondiffracting Pulses Next, we show how to get finite-energy localized wave pulses. These new waves can propagate long distances while maintaining their spatial resolution (i.e., they possess a large depth of field).

As we have seen, ideal nondiffracting waves can be constructed by superposing Bessel beams [Eq. (2.12) for cylindrical symmetry] with a spectrum $A(\omega, k_z)$ that satisfies a linear relationship between ω and k_z . In the general bidirectional decomposition method, this can be made by using spectra of the type (2.17) in superposition (2.15).

Solutions of this type possess an infinite depth of field; however, they also exhibit infinite energy [11,13]. To overcome this problem, we can truncate an ideal nondiffracting wave by a finite aperture, and the resulting pulse will have finite energy with finite field depths. Even so, these depths may be very large compared with those of ordinary waves. The problem in this case is that the resulting field has to be calculated from the diffraction integrals (such as the well-known Rayleigh–Sommerfeld

formula), and, in general, a closed analytical formula for the resulting pulse cannot be obtained.

However, there is another way to construct localized pulses with finite energy [13]: by using spectra $A(\omega, k_z)$ in (2.12) whose domains are not restricted to being defined exactly over the straight line $\omega = Vk_z + b$, but around that line, where the spectra should concentrate their main values. In other words, the spectrum has to be well localized in the vicinity of the line.

Similarly, in terms of the generalized bidirectional decomposition given in (2.15), finite-energy nondiffracting wave pulses can be constructed based on well-localized spectral functions $A(\alpha, \beta)$ in the vicinity of the line $\beta = \beta_0$, β_0 being a constant.

To exemplify this method, let us consider the spectrum

$$A(\alpha, \beta) = \begin{cases} aqV e^{-aV\alpha} e^{-q(\beta-\beta_0)} & \text{for } \beta \geq \beta_0 \\ 0 & \text{for } 0 \leq \beta < \beta_0 \end{cases} \quad (2.28)$$

in the superposition (2.15), a and q being free positive constants and V the peak's pulse velocity (here, $V \geq c$).

It is easy to see that the spectrum above is zero in the region above the $\beta = \beta_0$ line, while it decays in the region below (as well as along) such a line. We can concentrate this spectrum on $\beta = \beta_0$ by choosing values of q such that $q\beta_0 \gg 1$. The faster the spectrum decay takes place in the region below the $\beta = \beta_0$ line, the larger the field depth of the corresponding pulse.

Once we choose $q\beta_0 \gg 1$ to obtain pulses with a large depth of field, we can also minimize the contribution of the noncausal (backward) components by choosing $aV\beta_0 \ll 1$, in analogy with the results we obtained for the SFWM case.

Still in analogy with the SFWM case, when we choose $q\beta_0 \gg 1$ (i.e., long depth of field) and $aV\beta_0 \ll 1$ (minimal contribution of backward components), we can simplify the argument of the Bessel function in the integrand of superposition (2.15) by neglecting the term $(V^2/c^2 - 1)\beta_0^2$.

With the comments above, we can write the superposition (2.15) with the spectrum (2.28) as

$$\begin{aligned} \Psi(\rho, \zeta, \eta) \approx aqV \int_{\beta_0}^{\infty} d\beta \int_0^{\infty} d\alpha J_0 \left[\rho \sqrt{\left(\frac{V^2}{c^2} - 1\right) \alpha^2 + 2\left(\frac{V^2}{c^2} + 1\right) \alpha\beta} \right] \\ \times e^{-i\beta\eta} e^{i\alpha\zeta} e^{-q(\beta-\beta_0)} e^{-aV\alpha}, \end{aligned} \quad (2.29)$$

and using identity (6.616.1) in [19], we get

$$\Psi(\rho, \zeta, \eta) \approx qX \int_{\beta_0}^{\infty} d\beta e^{-q(\beta-\beta_0)} e^{-i\beta\eta} \exp \left[\beta \frac{V^2 + c^2}{V^2 - c^2} (aV - i\zeta - aVX^{-1}) \right], \quad (2.30)$$

which can be viewed as a superposition of the SFWM pulses [see Eq. (2.26)].

The integration above can be made easily and results [13] in the *superluminal modified power spectrum* (SMPS) pulse:

$$\Psi_{\text{SMPS}}(\rho, \zeta, \eta) = qX \frac{\exp[(Y - i\eta)\beta_0]}{q - (Y - i\eta)}, \quad (2.31)$$

where X is the ordinary X pulse (2.21) and Y is defined as

$$Y \equiv \frac{V^2 + c^2}{V^2 - c^2} [(aV - i\zeta) - aVX^{-1}]. \quad (2.32)$$

The SMPS pulse is a superluminal localized wave with field concentration around $\rho = 0$ and $\zeta = 0$ (i.e., in $z = Vt$) and with finite total energy. We will show that the depth of field, Z , of this pulse is given by $Z_{\text{SMPS}} = q/2$.

An interesting property of the SMPS pulse is related to its transverse width (the transverse spot size at the pulse center). It can be shown from (2.31) that for cases where $aV \ll 1/\beta_0$ and $q\beta_0 \gg 1$ (i.e., for the cases considered by us), the transverse spot size, $\Delta\rho$, of the pulse center ($\zeta = 0$) is dictated by the exponential function in (2.31) and is given by

$$\Delta\rho = c \sqrt{\frac{aV}{\beta_0(V^2 + c^2)} + \frac{V^2 - c^2}{4\beta_0^2(V^2 + c^2)^2}}, \quad (2.33)$$

which clearly does not depend on z , and so remains constant during the propagation. In other words, despite the fact that the SMPS pulse suffers an intensity decrease during the propagation, it preserves its transverse spot size. This interesting characteristic is not verified in ordinary pulses such as Gaussian pulses, where the amplitude of the pulse decreases and the width increases by the same factor.

Figure 2.1 shows a SMPS pulse intensity with $\beta_0 = 33 \text{ m}^{-1}$, $V = 1.01c$, $a = 10^{-12} \text{ s}$, and $q = 10^5 \text{ m}$ at two different moments, for $t = 0$ and after 50 km of propagation, where as we can see, the pulse becomes less intense (half of its initial peak intensity). It can be noted that despite the intensity decrease, the pulse maintains its transverse width, as we can see from the two-dimensional plots in Fig. 2.1, which show the field intensities in transverse sections at $z = 0$ and $z = q/2 = 50 \text{ km}$.

Three other important well-known finite-energy nondiffracting solutions can be obtained directly from the SMPS pulse. The first one, obtained from (2.31) by making $\beta_0 = 0$, is the *superluminal splash pulse* (SSP) [13],

$$\Psi_{\text{SSP}}(\rho, \zeta, \eta) = \frac{qX}{q + i\eta - Y}. \quad (2.34)$$

The other two are luminal pulses. By taking the limit $V \rightarrow c^+$ in the SMPS pulse (2.31) we get the well-known *luminal modified power spectrum* (MPS) pulse [11],

$$\Psi_{\text{MPS}}(\rho, \zeta, \eta) = \frac{aqce^{-i\beta_0\eta}}{(q + i\eta)(ac - i\zeta) + \rho^2} \exp\left(\frac{-\beta_0\rho^2}{ac - i\zeta}\right). \quad (2.35)$$

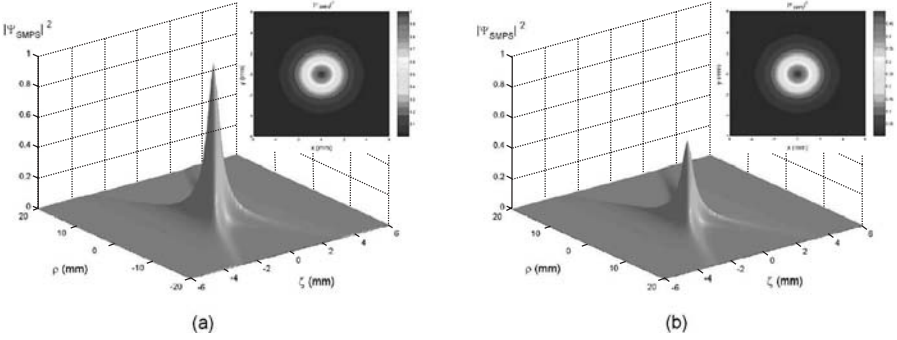


FIGURE 2.1 Representation of a superluminal modified power spectrum pulse, Eq. (2.31). Its total energy is finite (even without truncation), so it gets deformed while propagating, since its amplitude decreases with time. In (a) we represent for $t = 0$, the pulse corresponding to $\beta_0 = 33 \text{ m}^{-1}$, $V = 1.01c$, $a = 10^{-12} \text{ s}$, and $q = 10^5 \text{ m}$. The same pulse is depicted in (b) after having traveled 50 km.

Finally, by taking the limit $V \rightarrow c^+$ and making $\beta_0 = 0$ in the SMPS pulse [or equivalently, by making $\beta_0 = 0$ in the MPS pulse (2.35), or by taking the limit $V \rightarrow c^+$ in the SSP (2.34)], we obtain the well-known *luminal splash pulse* (SP) solution [11],

$$\Psi_{\text{SP}}(\rho, \zeta, \eta) = \frac{aqc}{(q + i\eta)(ac - i\zeta) + \rho^2}. \quad (2.36)$$

It is also interesting to note that the X and SFWM pulses can be obtained from the SSP and SMPS pulses (respectively) by making $q \rightarrow \infty$ in Eqs. (2.34) and (2.31). As a matter of fact, the solutions SSP and SMPS can be viewed as finite-energy versions of the X and SFWM, pulses, respectively.

Some Characteristics of the SMPS Pulse Let us examine the on-axis ($\rho = 0$) behavior of the SMPS pulse. On $\rho = 0$ we have

$$\Psi_{\text{SMPS}}(\rho = 0, \zeta, \eta) = aqVe^{-i\beta_0\zeta}[(aV - i\zeta)(q + i\eta)]^{-1}. \quad (2.37)$$

From this expression we can show that the longitudinal localization Δz , for $t = 0$, of the SMPS pulse square magnitude is

$$\Delta z = 2aV. \quad (2.38)$$

If we now define the field depth Z as the distance over which the pulse's peak intensity is 50% at least of its initial value,[†] we can obtain, from (2.37), the depth of field

$$Z_{\text{SMPS}} = \frac{q}{2}, \quad (2.39)$$

[†] We can expect that while the pulse peak intensity is maintained, so is its spatial form.

which depends solely on q , as we expected, since q regulates the concentration of the spectrum around the line $\omega = V k_z + 2V\beta_0$.

Now, let us examine the maximum amplitude M of the real part of (2.37), which for $z = Vt$ is written ($\zeta = 0$ and $\eta = 2z$)

$$M_{\text{SMPS}} \equiv \text{Re}[\Psi_{\text{SMPS}}(\rho = 0, z = Vt)] = \frac{\cos 2\beta_0 z - 2(z/q) \sin 2\beta_0 z}{1 + 4(z/q)^2}. \quad (2.40)$$

Initially, for $z = 0, t = 0$, one has $M = 1$ and can also infer that:

1. When $z/q \ll 1$ (i.e., when $z \ll Z$), Eq. (2.40) becomes

$$M_{\text{SMPS}} \approx \cos 2\beta_0 z \quad \text{for } z \ll Z \quad (2.41)$$

and the pulse's peak oscillates harmonically with "wavelength" $\Delta z_0 = \pi/\beta_0$ and "period" $\Delta t_0 = \pi/V\beta_0$, all along its field depth.

2. When $z/q \gg 1$ (i.e., $z \gg Z$), Eq. (2.40) becomes

$$M_{\text{SMPS}} \approx -\frac{\sin 2\beta_0 z}{2z/q} \quad \text{for } z \gg Z. \quad (2.42)$$

Therefore, beyond its depth of field, the pulse goes on oscillating with the same Δz_0 , but its maximum amplitude decays proportionally to z .

In the next two sections we look at an interesting application of localized wave pulses.

2.3 SPACE-TIME FOCUSING OF X-SHAPED PULSES

In this section we show how one can in general use any known superluminal solutions to obtain a large number of analytic expressions for space-time focused waves, endowed with a very strong intensity peak at the location desired. The method presented here is a natural extension of that developed by A. Shaarawi et al. [20], where space-time focusing was achieved by superimposing a discrete number of ordinary X-waves, characterized by different values of axicon angles θ .

In this section, we go on to more efficient superpositions [21] for varying velocities V , related to θ through the known [3,4] relation $V = c/\cos\theta$. This enhanced focusing scheme has the advantage of yielding analytic (closed-form) expressions for the spatiotemporally focused pulses.

Let us start by considering an axially symmetric ideal nondiffracting superluminal wave pulse $\psi(\rho, z - Vt)$ in a dispersionless medium, where $V = c/\cos\theta > c$ is the pulse velocity, with θ being the axicon angle. As we saw in Section 2.2, pulses like these can be obtained by a suitable frequency superposition of Bessel beams.

Suppose that we now have N waves of the type $\psi_n(\rho, z - V_n(t - t_n))$, with different velocities, $c < V_1 < V_2 < \dots < V_N$, emitted at (different) times t_n , quantities t_n being constants, while $n = 1, 2, \dots, N$. The center of each pulse is localized at $z = V_n(t - t_n)$. To obtain a highly focused wave, we need all wave components $\psi_n(\rho, z - V_n(t - t_n))$ to reach the point $z = z_f$ at the same time $t = t_f$. On choosing $t_1 = 0$ for the slowest pulse ψ_1 , it is easily seen that the peak of this pulse reaches the point $z = z_f$ at the time $t_f = z_f/V_1$. So for each ψ_n , the instant of emission t_n must be

$$t_n = \left(\frac{1}{V_1} - \frac{1}{V_n} \right) z_f. \quad (2.43)$$

With this we can construct other exact solutions to the wave equation given by [21]

$$\Psi(\rho, z, t) = \int_{V_{\min}}^{V_{\max}} dV A(V) \psi \left[\rho, z - V \left(t - \left(\frac{1}{V_{\min}} - \frac{1}{V} \right) z_f \right) \right], \quad (2.44)$$

where V is the velocity of the wave $\psi(\rho, z - Vt)$ in the integrand of (2.44). In the integration, V is considered as a continuous variable in the interval $[V_{\min}, V_{\max}]$. In Eq. (2.44), $A(V)$ is the velocity-distribution function that specifies the contribution to the integration of each wave component (with velocity V). The resulting wave $\Psi(\rho, z, t)$ can have a more or less strong amplitude peak at $z = z_f$ at time $t_f = z_f/V_{\min}$, depending on $A(V)$ and on the difference $V_{\max} - V_{\min}$. Let us notice that the resulting wave field will also propagate with a superluminal peak velocity, also depending on $A(V)$. When the velocity-distribution function is well concentrated around a certain velocity value, one can expect the wave (2.44) to increase its magnitude and spatial localization while propagating. Finally, as we know, the pulse peak acquires its maximum amplitude and localization at the chosen point $z = z_f$ and at time $t = z_f/V_{\min}$. Afterward the wave suffers progressive spreading and decrease in amplitude.

2.3.1 Focusing Effects Using Ordinary X-Waves

Here we present a specific example by integrating (2.44) over ordinary standard X-waves [40], $X = aV[(aV - i(z - Vt))^2 + (V^2/c^2 - 1)\rho^2]^{-1/2}$. When using this ordinary X-wave, the largest spectral amplitudes are obtained for low frequencies. For this reason, one may expect that the solutions considered below will be suitable mainly for low-frequency applications. Let us choose, then, the function ψ in the integrand of Eq. (2.44) to be $\psi(\rho, z, t) \equiv X(\rho, z - V(t - (1/V_{\min} - 1/V)z_f))$, that is,

$$\psi(\rho, z, t) \equiv X = \frac{aV}{\sqrt{[aV - i(z - V(t - (1/V_{\min} - 1/V)z_f))]^2 + (V^2/c^2 - 1)\rho^2}}. \quad (2.45)$$

After some manipulations, we obtain the analytic integral solution

$$\Psi(\rho, z, t) = \int_{V_{\min}}^{V_{\max}} \frac{aVA(V)}{\sqrt{PV^2 + QV + R}} dV, \quad (2.46)$$

with

$$\begin{aligned} P &= [a + i(t - z_f/V_{\min})]^2 + \rho^2/c^2 \\ Q &= 2(t - z_f/V_{\min} - ai)(z - z_f) \\ R &= -(z - z_f)^2 - \rho^2. \end{aligned} \quad (2.47)$$

In what follows we illustrate the behavior of some new spatiotemporally focused pulses by taking into consideration some different velocity distributions $A(V)$. These new pulses are closed analytical *exact* solutions of the wave equation.

Example 1 Let us consider our integral solution (2.46) with $A(V) = 1$ s/m. In this case the contribution of the X-waves is the same for all velocities in the range allowed, $[V_{\min}, V_{\max}]$. Using identity (2.264.2) of [19], we get the particular solution

$$\begin{aligned} \Psi(\rho, z, t) &= \frac{a}{P} \left(\sqrt{PV_{\max}^2 + QV_{\max} + R} - \sqrt{PV_{\min}^2 + QV_{\min} + R} \right) \\ &+ \frac{aQ}{2P^{3/2}} \ln \frac{2\sqrt{P(PV_{\min}^2 + QV_{\min} + R)} + 2PV_{\min} + Q}{2\sqrt{P(PV_{\max}^2 + QV_{\max} + R)} + 2PV_{\max} + Q}, \end{aligned} \quad (2.48)$$

where P , Q , and R are as given in Eq. (2.47). A three-dimensional plot of this function is provided in Fig. 2.2, where we have chosen $a = 10^{-12}$ s, $V_{\min} = 1.001c$, $V_{\max} = 1.005c$, and $z_f = 200$ cm. It can be seen that this solution exhibits a rather evident space–time focusing. An initially spread-out pulse (shown for $t = 0$) becomes highly localized at $t = t_f = z_f/V_{\min} = 6.66$ ns, the pulse peak amplitude at z_f being 40.82 times greater than the initial one. In addition, at the focusing time t_f , the field is much more localized than at any other times. The velocity of this pulse is approximately $V = 1.003c$.

Example 2 In this case we choose $A(V) = 1/V$ (s/m), and using the identity (2.261) of [19], Eq. (2.46) gives

$$\Psi(\rho, z, t) = \frac{a}{\sqrt{P}} \ln \frac{2\sqrt{P(PV_{\max}^2 + QV_{\max} + R)} + 2PV_{\max} + Q}{2\sqrt{P(PV_{\min}^2 + QV_{\min} + R)} + 2PV_{\min} + Q}. \quad (2.49)$$

Other exact closed solutions can be obtained [21] considering, for instance, velocity distributions as $A(V) = 1/V^2$ and $A(V) = 1/V^3$.

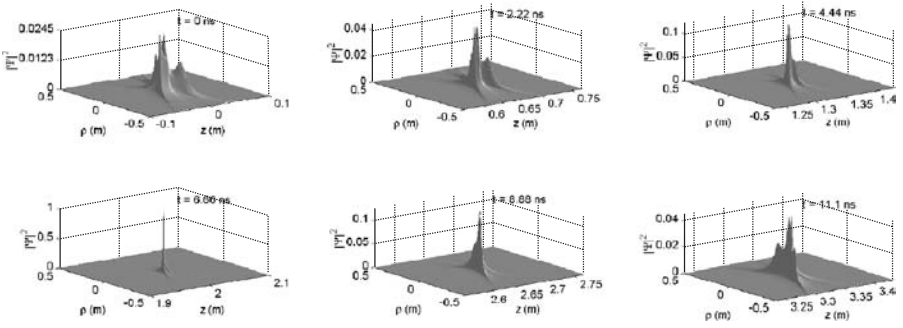


FIGURE 2.2 Space–time evolution of the superluminal pulse represented by Eq. (2.48); the parameter chosen values are $a = 10^{-12}$ s, $V_{\min} = 1.001c$, and $V_{\max} = 1.005c$, and the focusing point is at $z_f = 200$ cm. One can see that this solution is associated with rather good spatiotemporal focusing. The field amplitude at $z = z_f$ is 40.82 times larger than the initial amplitude. The field amplitude is normalized at the space–time point $\rho = 0$, $z = z_f$, $t = t_f$.

Actually, we can construct many others spatiotemporally focused pulses from the foregoing solutions just by taking time derivatives (of any order). It is also possible to show [21] that the new solutions obtained in this way have their spectra shifted toward higher frequencies.

2.4 CHIRPED OPTICAL X-TYPE PULSES IN MATERIAL MEDIA

The theory of the localized waves was developed initially for free space (vacuum). In 1996, Sõnajalg and Saari [5] showed that the localized wave theory can be extended to include (unbounded) dispersive media. This was obtained by making the axicon angle of Bessel beams (BBs) vary with the frequency [5–7] in such a way that a suitable frequency superposition of these beams compensates for the material dispersion. Soon after this idea was reported, many interesting nondiffracting/nondispersive pulses were obtained theoretically [5–7] and experimentally [5].

Despite this extended method being of remarkable importance, working well in theory, its experimental implementation is not so simple.[†] In 2004, Zamboni-Rached et al. [22] developed a simpler way to obtain pulses capable of recovering their spatial shape, both transversally and longitudinally, after some propagation. It consists of using chirped optical X-type pulses while keeping the axicon angle fixed. Let us recall that, by contrast, chirped Gaussian pulses in unbounded material media may recover only their longitudinal shape, since they undergo a progressive transverse spreading while propagating. The present section is devoted to this approach.

Let us start with an axially-symmetric Bessel beam in a material medium with refractive index $n(\omega)$:

$$\psi(\rho, z, t) = J_0(k_\rho \rho) \exp(i\beta z) \exp(-i\omega t), \quad (2.50)$$

[†] We refer interested readers to [5–7] to obtain a description, theoretical and experimental, of this extended method.

which must obey the condition $k_\rho^2 = n^2(\omega)\omega^2/c^2 - \beta^2$, which connects the transverse and longitudinal wave numbers k_ρ and β and the angular frequency ω . In addition, we impose the conditions that $k_\rho^2 \geq 0$ and $\omega/\beta \geq 0$, to avoid the nonphysical behavior of the Bessel function $J_0(\cdot)$ and to confine ourselves to forward propagation.

Once the conditions above are satisfied, we have the liberty of writing the longitudinal wave number as $\beta = [n(\omega)\omega\cos\theta]/c$, and therefore, $k_\rho = [n(\omega)\omega\sin\theta]/c$, where (as in the free-space case) θ is the axicon angle of the Bessel beam.

Now we can obtain a X-shaped pulse by performing a frequency superposition of these BBs, with β and k_ρ given by the previous relations:

$$\Psi(\rho, z, t) = \int_{-\infty}^{\infty} S(\omega) J_0\left(\frac{n(\omega)\omega}{c} \sin\theta \rho\right) \exp[i\beta(\omega)z] \exp(-i\omega t) d\omega, \quad (2.51)$$

where $S(\omega)$ is the frequency spectrum and the axicon angle is kept constant.

One can see that the phase velocity of each BB in our superposition (2.51) is different and is given by $V_{\text{phase}} = c/[n(\omega)\cos\theta]$, so the pulse given by (2.51) will suffer dispersion during its propagation.

As we said, the method developed by Sönajalg and Saari [5] and explored by others [6,7] to overcome this problem consisted of regarding the axicon angle θ as a function of the frequency, in order to obtain a linear relationship between β and ω . Here, however, we wish to work with a *fixed* axicon angle, and we have to find another way to avoid dispersion and diffraction along a certain propagation distance. To do that, we might choose a chirped Gaussian spectrum $S(\omega)$ in Eq. (2.51):

$$S(\omega) = \frac{T_0}{\sqrt{2\pi(1+iC)}} \exp[-q^2(\omega - \omega_0)^2] \quad \text{with } q^2 = \frac{T_0^2}{2(1+iC)}, \quad (2.52)$$

where ω_0 is the central frequency of the spectrum, T_0 is a constant related to the initial temporal width, and C is the chirp parameter (we chose as a temporal width the half-width of the relevant Gaussian curve when its height equals $1/e$ times its full height). Unfortunately, there is no analytical solution to Eq. (2.51) with $S(\omega)$ given by Eq. (2.52), so some approximations must be made.

Then, let us assume that the spectrum $S(\omega)$ surrounding the carrier frequency ω_0 is narrow enough that $\Delta\omega/\omega_0 \ll 1$, to ensure that $\beta(\omega)$ can be approximated by the first three terms of its Taylor expansion in the vicinity of ω_0 ; that is, $\beta(\omega) \approx \beta(\omega_0) + \beta'(\omega)|_{\omega_0}(\omega - \omega_0) + (1/2)\beta''(\omega)|_{\omega_0}(\omega - \omega_0)^2$, where after using $\beta = [n(\omega)\omega\cos\theta]/c$,

$$\frac{\partial\beta}{\partial\omega} = \frac{\cos\theta}{c} \left[n(\omega) + \omega \frac{\partial n}{\partial\omega} \right], \quad \frac{\partial^2\beta}{\partial\omega^2} = \frac{\cos\theta}{c} \left(2 \frac{\partial n}{\partial\omega} + \omega \frac{\partial^2 n}{\partial\omega^2} \right). \quad (2.53)$$

As we know, $\beta'(\omega)$ is related to the pulse group velocity by the relation $Vg = 1/\beta'(\omega)$. Here we can see the difference between the group velocity of an X-type pulse (with a fixed axicon angle) and that of a standard Gaussian pulse. Such a difference is due to the factor $\cos\theta$ in Eq. (2.53). Because of it, the group velocity

of our X-type pulse is always greater than that of a Gaussian pulse. In other words, $(V_g)_X = (1/\cos\theta)(V_g)_{\text{gauss}}$.

We also know that the second derivative of $\beta(\omega)$ is related to the group-velocity dispersion (GVD) β_2 by $\beta_2 = \beta''(\omega)$. The GVD is responsible for the temporal (longitudinal) spreading of the pulse. Here one can see that the GVD of the X-type pulse is always smaller than that of standard Gaussian pulses, due to the factor $\cos\theta$ in Eq. (2.53): namely, $(\beta_2)_X = \cos\theta(\beta_2)_{\text{Gauss}}$.

Using the results above, we can write

$$\Psi(\rho, z, t) = \frac{T_0 \exp[i\beta(\omega_0)z] \exp(-i\omega_0 t)}{\sqrt{2\pi(1+iC)}} \int_{-\infty}^{\infty} d\omega J_0 \left[\frac{n(\omega)\omega}{c} \sin\theta \rho \right] \\ \times \exp \left[i \frac{\omega - \omega_0}{V_g} (z - V_g t) \right] \exp \left[(\omega - \omega_0)^2 \left(\frac{i\beta_2}{2} z - q^2 \right) \right]. \quad (2.54)$$

The integral in Eq. (2.54) cannot be solved analytically, but it is enough for us to obtain the pulse behavior. Let us analyze the pulse for $\rho = 0$. In this case we obtain

$$\Psi(\rho = 0, z, t) = \frac{T_0 \exp[i\beta(\omega_0)z] \exp(-i\omega_0 t)}{\sqrt{T_0^2 - i\beta_2(1+iC)z}} \exp \left[\frac{-(z - V_g t)^2(1+iC)}{2V_g^2[T_0^2 - i\beta_2(1+iC)z]} \right]. \quad (2.55)$$

From Eq. (2.55) we can see immediately that the initial temporal width of the pulse intensity is T_0 and that after some propagation distance z , the time width T_1 becomes

$$\frac{T_1}{T_0} = \left[\left(1 + \frac{C\beta_2 z}{T_0^2} \right)^2 + \left(\frac{\beta_2 z}{T_0^2} \right)^2 \right]^{1/2}. \quad (2.56)$$

Relation (2.56) describes the pulse spreading behavior. One can easily show that such behavior depends on the sign (positive or negative) of product $\beta_2 C$, as is well known for standard Gaussian pulses [23].

When $\beta_2 C > 0$, the pulse will become broader and broader monotonically with distance z . On the other hand, if $\beta_2 C < 0$, in the first stage, the pulse will suffer a narrowing and then will spread during the remainder of its propagation. So there will be a certain propagation distance in which the pulse will recover its initial temporal width ($T_1 = T_0$). From relation (2.56) we can find this distance $Z_{T_1=T_0}$ (given that $\beta_2 C < 0$) to be

$$Z_{T_1=T_0} = \frac{-2CT_0^2}{\beta_2(C^2 + 1)}. \quad (2.57)$$

One may notice that the maximum distance at which our chirped pulse, with given T_0 and β_2 , may recover its initial temporal width can be evaluated easily from Eq. (2.57) and results in $L_{\text{disp}} = T_0^2/\beta_2$. We call such a maximum value L_{disp} the dispersion length. It is an maximum distance an X-type pulse may travel while

recovering its initial longitudinal shape. Obviously, if we want the pulse to re-assume its longitudinal shape at some desired distance $z < L_{\text{disp}}$, we have simply to choose a suitable value of the chirp parameter.

Let us emphasize that the property of recovering its own initial temporal (or longitudinal) width may also be verified to exist in the case of chirped standard Gaussian pulses. However, the latter will suffer a progressive transverse spreading which will not be reversible. The distance at which a Gaussian pulse doubles its initial transverse width w_0 is $z_{\text{diff}} = \sqrt{3} \pi w_0^2 / \lambda_0$, where λ_0 is the carrier wavelength. Thus, we can see that optical Gaussian pulses with great transverse localization will get spoiled in a few centimeters or even less.

Next we show that it is also possible to recover the transverse shape of the chirped X-type pulse intensity; actually, it is possible to recover its entire spatial shape after a distance $Z_{T_1=T_0}$. To see this, let us go back to our integral solution (2.54), and perform the change of coordinates $(z, t) \rightarrow (\Delta z, t_c = z_c / V_g)$, with

$$z = z_c + \Delta z, \quad t = t_c \equiv \frac{z_c}{V_g}, \quad (2.58)$$

where z_c is the center of the pulse (Δz is the distance from such a point) and t_c is the time at which the pulse center is located at z_c . In this way, $\Psi(\rho, z, t)$ becomes $\Psi(\rho, t_c + \Delta z, z_c / V_g)$; that is, $\Psi(\rho, z_c, \Delta z)$. We are going to compare our integral solution (2.54) when $z_c = 0$ (initial pulse) with that when $z_c = Z_{T_1=T_0} = -2CT_0^2 / [\beta_2(C_2 + 1)]$. In this way, the solution (2.54) can be written, when $z_c = 0$, as

$$\begin{aligned} \Psi(\rho, z_c = 0, \Delta z) &= \frac{T_0 \exp(i\beta_0 \Delta z)}{\sqrt{2\pi(1+iC)}} \int_{-\infty}^{\infty} d\omega J_0(k_\rho(\omega)\rho) \exp\left[\frac{-T_0^2(\omega - \omega_0)^2}{2(1+C^2)}\right] \\ &\times \exp\left\{i\left[\frac{(\omega - \omega_0)\Delta z}{V_g} + \frac{(\omega - \omega_0)^2\beta_2\Delta z}{2} + \frac{(\omega - \omega_0)^2T_0^2C}{2(1+C^2)}\right]\right\}, \end{aligned} \quad (2.59)$$

where we have taken the value q given by (2.52).

To verify that the pulse intensity recovers its entire original form at $z_c = Z_{T_1=T_0} = -2CT_0^2 / [\beta_2(C^2 + 1)]$, we can analyze our integral solution at that point, obtaining

$$\begin{aligned} \Psi(\rho, z_c = Z_{T_1=T_0}, \Delta z) &= \frac{T_0 \exp\left\{i\beta_0\left[z_c - \Delta z' - \frac{cz_c}{\cos\theta n(\omega_0)V_g}\right]\right\}}{\sqrt{2\pi(1+iC)}} \\ &\times \int_{-\infty}^{\infty} d\omega J_0(k_\rho(\omega)\rho) \exp\left[\frac{-T_0^2(\omega - \omega_0)^2}{2(1+C^2)}\right] \\ &\times \exp\left\{-i\left[\frac{(\omega - \omega_0)\Delta z'}{V_g} + \frac{(\omega - \omega_0)^2\beta_2\Delta z'}{2} + \frac{(\omega - \omega_0)^2T_0^2C}{2(1+C^2)}\right]\right\}, \end{aligned} \quad (2.60)$$

where we put $\Delta z = -\Delta z'$. In this way, we see immediately that

$$|\Psi(\rho, z_c = 0, \Delta z)|^2 = |\Psi(\rho, z_c = Z_{T_1=T_0}, -\Delta z)|^2. \quad (2.61)$$

Therefore, from Eq. (2.61) it is clear that the chirped optical X-type pulse intensity will recover its original three-dimensional form, with just a longitudinal inversion at the pulse center: the present method being, in this way, a simple and effective procedure for compensating the effects of diffraction and dispersion in an unbounded material medium and a method simpler than that of varying the axicon angle with the frequency. Let us stress that we can choose the distance $z = Z_{T_1=T_0} \leq L_{\text{disp}}$ at which the pulse will again take on its spatial shape by choosing a suitable value of the chirp parameter.

Up to now we have shown that the chirped X-type pulse recovers its three-dimensional shape after some distance, and we have also obtained an analytical description of the pulse longitudinal behavior (for $\rho = 0$) during propagation, by means of Eq. (2.56). However, we do not get the same information about pulse transverse behavior: We just know that it is recovered at $z = Z_{T_1=T_0}$.

So, to complete the picture, it would be interesting if we could also find the transverse behavior in the plane of the pulse center $z = V_g t$. In that way we would obtain quantitative information about the evolution of the pulse shape during its entire propagation. We do not examine the mathematical details here; we just affirm that transverse behavior of the pulse (in the plane $z = z_c = V_g t$) during its entire propagation can be described approximately by

$$\begin{aligned} & \Psi \left(\rho, z = z_c, t = \frac{z_c}{V_g} \right) \\ & \approx \frac{T_0 \exp[i\beta(\omega_0)z] \exp(-i\omega_0 t) \exp\left[(-\tan^2 \theta \rho^2)/8V_g^2(-i\beta_2 z_c/2 + q^2)\right]}{\sqrt{2\pi(1+iC)} \sqrt{-i\beta_2 z_c/2 + q^2}} \\ & \times \left[\Gamma(1/2) J_0 \left(\frac{n(\omega_0)\omega_0 \sin \theta \rho}{c} \right) I_0 \left(\frac{\tan^2 \theta \rho^2}{8V_g^2(-i\beta_2 z_c/2 + q^2)} \right) \right. \\ & + 2 \sum_{p=1}^{\infty} \frac{2^p \Gamma(p+1/2)\Gamma(p+1)}{\Gamma(2p+1)} J_{2p} \left(\frac{n(\omega_0)\omega_0 \sin \theta \rho}{c} \right) \\ & \left. \times I_{2p} \left(\frac{\tan^2 \theta \rho^2}{8V_g^2(-i\beta_2 z_c/2 + q^2)} \right) \right], \quad (2.62) \end{aligned}$$

where $I_p(\cdot)$ is the modified Bessel function of the first kind of order p , the quantity $\Gamma(\cdot)$ being the gamma function and q given by (2.52). The interested reader may consult [22] for details on how to obtain Eq. (2.62) from Eq. (2.54). At first glance this solution could appear to be very complicated, but *the series on its right-hand side provides a negligible contribution*. This fact renders our solution (2.62) of important practical interest and we use it in the following.

For additional information about the transverse pulse evolution [extracted from Eq. (2.62)] reader's are referred to [22], where the effects of finite aperture generation on chirped X-type pulses are analyzed.

2.4.1 Example: Chirped Optical X-Type Pulse in Bulk Fused Silica

For bulk fused silica, the refractive index $n(\omega)$ can be approximated by the Sellmeier equation [23],

$$n^2(\omega) = 1 + \sum_{j=1}^N \frac{B_j \omega_j^2}{\omega_j^2 - \omega^2}, \tag{2.63}$$

where ω_j are the resonance frequencies, B_j the strength of the j th resonance, and N the total number of material resonances that appear in the frequency range of interest. For our purposes it is appropriate to choose $N = 3$, which yields for bulk fused silica [23] the values $B_1 = 0.6961663$, $B_2 = 0.4079426$, $B_3 = 0.8974794$, $\lambda_1 = 0.0684043 \mu\text{m}$, $\lambda_2 = 0.1162414 \mu\text{m}$, and $\lambda_3 = 9.896161 \mu\text{m}$.

Now, let us consider in this medium a chirped X-type pulse with $\lambda_0 = 0.2 \mu\text{m}$, $T_0 = 0.4 \text{ ps}$, $C = -1$, and an axicon angle $\theta = 0.00084 \text{ rad}$, which correspond to an initial central spot with $\Delta\rho_0 = 0.117 \text{ mm}$. From Eqs. (2.56) and (2.62) we get the longitudinal and transverse pulse evolution, which are represented in Fig. 2.3.

From Fig. 2.3a we note that initially, the pulse suffers a longitudinal narrowing with increased intensity up to the position $z = T_0^2/2\beta_2 = 0.186 \text{ m}$. After this point the pulse starts to broaden, decreasing its intensity and recovering its entire longitudinal shape (width and intensity) at the point $z = T_0^2/\beta_2 = 0.373 \text{ m}$, as was predicted. At the same time, from Fig. 2.3b we note that the pulse maintains its transverse width $\Delta\rho = 2.4 c/[n(\omega_0)\omega_0 \sin \theta] = 0.117 \text{ mm}$ (because $T_0\omega_0 \gg 1$) during its entire propagation; however, the same does not occur with pulse intensity. Initially, the

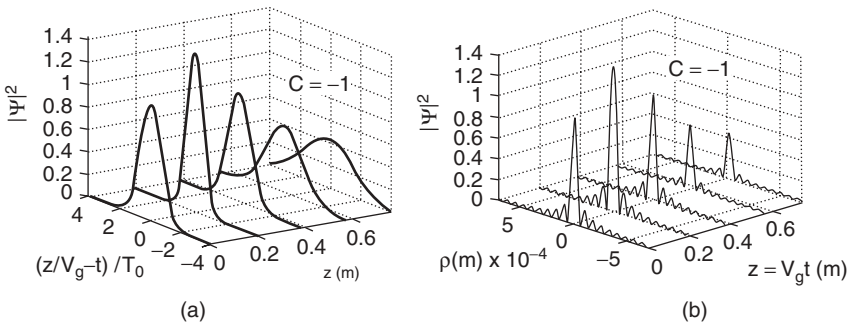


FIGURE 2.3 (a) Longitudinal-shape evolution of a chirped X-type pulse propagating in fused silica with $\lambda_0 = 0.2 \mu\text{m}$, $T_0 = 0.4 \text{ ps}$, $C = -1$, and axicon angle $\theta = 0.00084 \text{ rad}$, which correspond to an initial transverse width of $\Delta\rho_0 = 0.117 \text{ mm}$. (b) Transverse-shape evolution for the same pulse.

pulse suffers increased intensity up to the position $z_c = T_0^2/2\beta_2 = 0.186$ m; after this point, the intensity begins to decrease, and the pulse recovers its entire transverse shape at the point $z_c = T_0^2/\beta_2 = 0.373$ m, as we expected. Here we have skipped the series on the right-hand side of Eq. (2.62), because as we said earlier, it yields a negligible contribution.

Summarizing, from Fig. 2.3 we can see that the chirped X-type pulse recovers its longitudinal and transverse shape totally at the position $z = L_{\text{disp}} = T_0^2/\beta_2 = 0.373$ m, as we expected. Let us remember that a chirped Gaussian pulse may just recover its longitudinal width, but with an intensity decrease, at the position given by $z = Z_{T_1=T_0} = L_{\text{disp}} = T_0^2/\beta_2$. Its transverse width, on the other hand, suffers progressive and irreversible spreading.

2.5 MODELING THE SHAPE OF STATIONARY WAVE FIELDS: FROZEN WAVES

In this section we develop a very simple method [10,16,17] using superposition of forward propagating and equal-frequency Bessel beams that allows us to control the beam-intensity longitudinal shape within a chosen interval $0 \leq z \leq L$, where z is the propagation axis and L can be much greater than the wavelength λ of the monochromatic light (or sound) that is being used. Inside such a space interval, indeed, we succeed in constructing a stationary envelope whose longitudinal intensity pattern can assume any approximate shape desired, including, for instance, one or more high-intensity peaks, which is also naturally endowed with a good transverse localization. Since the intensity envelopes remains static (i.e., with velocity $V = 0$), we call such new solutions [10,16,17] to the wave equations *frozen waves*.

Although we are dealing here with exact solutions of the scalar wave equation, vectorial solutions of the same type can be obtained for the electromagnetic field, since solutions to Maxwell's equations follow naturally from scalar wave equation solutions [24,25]. We first present a method involving lossless media [16,17] and then extend the method to absorbing media [10].

2.5.1 Stationary Wave Fields with Arbitrary Longitudinal Shape in Lossless Media Obtained by Superposing Equal-Frequency Bessel Beams

We begin with the well-known axially-symmetric zeroth-order Bessel beam solution to the wave equation,

$$\psi(\rho, z, t) = J_0(k_\rho \rho) e^{i\beta z} e^{-i\omega t}, \quad (2.64)$$

with

$$k_\rho^2 = \frac{\omega^2}{c^2} - \beta^2, \quad (2.65)$$

where ω , k_ρ , and β are the angular frequency and the transverse and longitudinal wave numbers, respectively. We also impose the conditions

$$\frac{\omega}{\beta} > 0 \quad \text{and} \quad k_\rho^2 \geq 0 \quad (2.66)$$

(which imply that $\omega/\beta \geq c$) to ensure forward propagation only (with no evanescent waves), as well as the physical behavior of the Bessel function J_0 .

Now let us make a superposition of $2N + 1$ Bessel beams with the same frequency ω_0 but with different (and still unknown) longitudinal wave numbers β_m :

$$\Psi(\rho, z, t) = e^{-i\omega_0 t} \sum_{m=-N}^N A_m J_0(k_{\rho m} \rho) e^{i\beta_m z}, \quad (2.67)$$

where m represents integer numbers and the A_m are constant coefficients. For each m , the parameters ω_0 , $k_{\rho m}$, and β_m must satisfy (2.65), and, because of conditions (2.66), when considering $\omega_0 > 0$, we must have

$$0 \leq \beta_m \leq \frac{\omega_0}{c}. \quad (2.68)$$

Let us now suppose that we wish $|\Psi(\rho, z, t)|^2$, given by Eq. (2.67), to assume on the axis $\rho = 0$ the pattern represented by a function $|F(z)|^2$ inside the chosen interval $0 \leq z \leq L$. In this case, the function $F(z)$ can be expanded, as usual, in a Fourier series:

$$F(z) = \sum_{m=-\infty}^{\infty} B_m e^{i(2\pi/L)mz},$$

where

$$B_m = \frac{1}{L} \int_0^L F(z) e^{-i(2\pi/L)mz} dz.$$

More precisely, our goal is to find the values of the longitudinal wave numbers β_m and the coefficients A_m of (2.67) in order to reproduce approximately, within the interval $0 \leq z \leq L$ (for $\rho = 0$), the predetermined longitudinal intensity pattern $|F(z)|^2$. That is, we wish to have

$$\left| \sum_{m=-N}^N A_m e^{i\beta_m z} \right|^2 \approx |F(z)|^2 \quad \text{with } 0 \leq z \leq L. \quad (2.69)$$

Looking at Eq. (2.69), one might be tempted to take $\beta_m = 2\pi m/L$, thus obtaining a truncated Fourier series, expected to represent approximately the desired pattern $F(z)$. Superpositions of Bessel beams with $\beta_m = 2\pi m/L$ have actually been used

in some work to obtain a large set of *transverse* amplitude profiles [26]. However, for our purposes, this choice is not appropriate, for two principal reasons: (1) It yields negative values for β_m (when $m < 0$), which implies backward-propagating components (since $\omega_0 > 0$); and (2) when $L \gg \lambda_0$, which is of interest here, the main terms of the series would correspond to very small values of β_m , which results in a very short depth of field of the corresponding Bessel beams (when generated by finite apertures), preventing creation of the desired envelopes far from the source.

Therefore, we need to make a choice for the values of β_m that permits forward propagation components only and a good depth of field. This problem can be solved by putting

$$\beta_m = Q + \frac{2\pi}{L} m, \quad (2.70)$$

where $Q > 0$ is a value to be chosen (as we shall see) according to the given experimental situation and the desired degree of transverse field localization. Due to Eq. (2.68), we get

$$0 \leq Q \pm \frac{2\pi}{L} N \leq \frac{\omega_0}{c}. \quad (2.71)$$

Inequality (2.71) can be used to determine the maximum value of m , which we call N_{\max} , once Q , L , and ω_0 have been chosen.

As a consequence, to get a longitudinal intensity pattern approximately equal to the one desired, $|F(z)|^2$, in the interval $0 \leq z \leq L$, Eq. (2.67) should be rewritten as

$$\Psi(\rho = 0, z, t) = e^{-i\omega_0 t} e^{iQz} \sum_{m=-N}^N A_m e^{i(2\pi/L)mz}, \quad (2.72)$$

with

$$A_m = \frac{1}{L} \int_0^L F(z) e^{-i(2\pi/L)mz} dz. \quad (2.73)$$

Obviously, one obtains only an approximation to the desired longitudinal pattern, because the trigonometric series (2.72) is necessarily truncated ($N \leq N_{\max}$). Its total number of terms, let us repeat, will be fixed once the values of Q , L , and ω_0 are chosen.

When $\rho \neq 0$, the wave field $\Psi(\rho, z, t)$ becomes

$$\Psi(\rho, z, t) = e^{-i\omega_0 t} e^{iQz} \sum_{m=-N}^N A_m J_0(k_{\rho m} \rho) e^{i(2\pi/L)mz}, \quad (2.74)$$

with

$$k_{\rho m}^2 = \omega_0^2 - \left(Q + \frac{2\pi m}{L} \right)^2. \quad (2.75)$$

The coefficients A_m will yield the amplitudes and relative phases of each Bessel beam in the superposition.

Because we are adding together zero-order Bessel functions, we can expect a high field concentration around $\rho = 0$. Moreover, due to the known nondiffractive behavior of Bessel beams, we expect that the resulting wave field will preserve its transverse pattern in the entire interval $0 \leq z \leq L$.

The methodology developed here deals with longitudinal intensity pattern control. Obviously, we cannot get total three-dimensional control, due to the fact that the field must obey the wave equation. However, to have some control also over the transverse behavior, we can use two methods. The first is through the parameter Q of Eq. (2.70). Actually, we have some freedom in the choice of this parameter, and frozen waves representing the same longitudinal intensity pattern can possess different values of Q . The important point is that in superposition (2.74), using a smaller value of Q makes the Bessel beams possess a higher transverse concentration (because decreasing the value of Q increases the value of the Bessel beams transverse wave numbers), and this will be reflected in the resulting field, which will present a narrower central transverse spot. The second way to control the transverse intensity pattern is using higher-order Bessel beams, and we show this later.

Next, we look at a few examples of our methodology.

Example 1 Let us imagine that we have an optical wave field with $\lambda_0 = 0.632 \mu\text{m}$ (i.e., with $\omega_0 = 2.98 \times 10^{15}$ Hz), whose longitudinal pattern (along its z -axis) in the range $0 \leq z \leq L$ is given by the function

$$F(z) = \begin{cases} -4 \frac{(z - l_1)(z - l_2)}{(l_2 - l_1)^2} & \text{for } l_1 \leq z \leq l_2 \\ 1 & \text{for } l_3 \leq z \leq l_4 \\ -4 \frac{(z - l_5)(z - l_6)}{(l_6 - l_5)^2} & \text{for } l_5 \leq z \leq l_6 \\ 0 & \text{elsewhere,} \end{cases} \quad (2.76)$$

where $l_1 = L/5 - \Delta z_{12}$ and $l_2 = L/5 + \Delta z_{12}$ with $\Delta z_{12} = L/50$, $l_3 = L/2 - \Delta z_{34}$ and $l_4 = L/2 + \Delta z_{34}$ with $\Delta z_{34} = L/10$, and $l_5 = 4L/5 - \Delta z_{56}$ and $l_6 = 4L/5 + \Delta z_{56}$ with $\Delta z_{56} = L/50$. In other words, the longitudinal shape desired, in the range $0 \leq z \leq L$, is a parabolic function for $l_1 \leq z \leq l_2$, a unitary step function for $l_3 \leq z \leq l_4$, and a parabola again in the interval $l_5 \leq z \leq l_6$, being zero elsewhere (within the interval $0 \leq z \leq L$, as we said). In this example, let us put $L = 0.2$ m.

We can then easily calculate the coefficients A_m in the superposition (2.74), by inserting (2.76) into (2.73). Let us choose, for instance, $Q = 0.999 \omega_0/c$. This choice permits the maximum value $N_{\text{max}} = 316$ for m , as one can infer from Eq. (2.71). Let

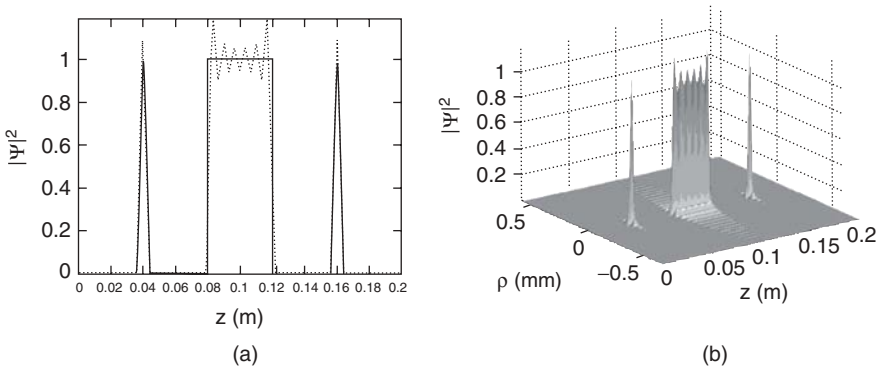


FIGURE 2.4 (a) Comparison of the intensity of the desired longitudinal function $F(z)$ and that of our frozen wave (FW), $\Psi(\rho = 0, z, t)$, obtained from Eq. (2.72). The solid line represents the function $F(z)$, and the dotted line our FW. (b) Three-dimensional plot of the field intensity of the FW chosen by us.

us emphasize that one is not compelled to use only $N = 316$, but can adopt for N any values *smaller* than 316: more generally, any value smaller than that calculated via inequality (2.71). Of course, using the maximum value allowed for N , one gets a better result.

In the present case, let us adopt the value $N = 30$. In Fig. 2.4a we compare the intensity of the longitudinal function $F(z)$ desired with that of the frozen wave, $\Psi(\rho = 0, z, t)$, obtained from Eq. (2.72) by adopting the value $N = 30$. One can verify that good agreement between the longitudinal behavior desired and our approximate FW is obtained with $N = 30$; the use of higher values only improves the approximation. Figure 2.4b shows the three-dimensional intensity of our FW, given by Eq. (2.74). One can observe that this field possesses the longitudinal pattern desired while being endowed with good transverse localization.

Example 2 We use this example to address an important concern. We can expect that for a desired longitudinal field intensity pattern, by choosing smaller values of the parameter Q , one will get FWs with a narrower transverse width [for the same number of terms in the series entering Eq. (2.74)], because the Bessel beams in Eq. (2.74) will possess larger transverse wave numbers, and consequently, higher transverse concentrations. We can verify this expectation by considering inside the usual range $0 \leq z \leq L$ the longitudinal pattern represented by the function

$$F(z) = \begin{cases} -4 \frac{(z - l_1)(z - l_2)}{(l_2 - l_1)^2} & \text{for } l_1 \leq z \leq l_2 \\ 0 & \text{elsewhere,} \end{cases} \quad (2.77)$$

with $l_1 = L/2 - \Delta z$ and $l_2 = L/2 + \Delta z$. Such a function has a parabolic shape with its peak centered at $L/2$ and with longitudinal width $2\Delta z/\sqrt{2}$. By adopting

$\lambda_0 = 0.632 \mu\text{m}$ (i.e., $\omega_0 = 2.98 \times 10^{15}$ Hz), let us use superposition (2.74) with two different values of Q : We shall obtain two different FWs that despite having the same longitudinal intensity pattern, possess different transverse localizations. Namely, let us consider $L = 0.06$ m and $\Delta z = L/100$ and the two values $Q = 0.999 \omega_0/c$ and $Q = 0.995 \omega_0/c$. In both cases the coefficients A_m will be the same, calculated from Eq. (2.73), this time using the value $N = 45$ in superposition (2.74). The results are shown in Fig. 2.5a and b. Both FWs have the same longitudinal intensity pattern, but the one with the smaller Q is endowed with a narrower transverse width.

With this, we can get some control on the transverse spot size through the parameter Q . Actually, Eq. (2.74), which defines our FW, is a superposition of zero-order Bessel beams, and due to this fact, the resulting field is expected to possess a transverse localization around $\rho = 0$. Each Bessel beam in superposition (2.74) is associated with a central spot with transverse size, or width, $\Delta\rho_m \approx 2.4/k_{\rho m}$. On the basis of the convergence of series (2.74) expected, we can estimate the width of the transverse spot of the resulting beam as being

$$\Delta\rho \approx \frac{2.4}{k_{\rho m=0}} = \frac{2.4}{\sqrt{\omega_0^2/c^2 - Q^2}}, \quad (2.78)$$

which is the same value as that for the transverse spot of the Bessel beam with $m = 0$ in superposition (2.74). Relation (2.78) can be useful: Once we have chosen the longitudinal intensity pattern desired, *we can even choose the size of the transverse spot and use relation (2.78) to evaluate the needed corresponding value of parameter Q .*

For more detailed analysis of the spatial resolution and residual intensity of frozen waves, we refer readers to [17].

Increasing Control of the Transverse Shape Using Higher-Order Bessel Beams

Here we argue that it is possible to increase our control of the transverse shape even more by using higher-order Bessel beams in our fundamental superposition (2.74). This new approach can be understood and accepted on the basis of simple and intuitive arguments, which are presented in [17]. A brief description of that approach follows.

The basic idea is to obtain the desired longitudinal intensity pattern not along the axis $\rho = 0$ but on a cylindrical surface corresponding to $\rho = \rho' > 0$. To do this, we proceed as before: Once we have chosen the longitudinal intensity pattern $F(z)$ desired, within the interval $0 \leq z \leq L$, we calculate the coefficients A_m as before [i.e., $A_m = (1/L) \int_0^L F(z) \exp(-i2\pi mz/L) dz$] and $k_{\rho m} = \sqrt{\omega_0^2 - (Q + 2\pi m/L)^2}$. Then we replace the zero-order Bessel beams $J_0(k_{\rho m}\rho)$, in superposition (2.74) with higher-order Bessel beams, $J_\mu(k_{\rho m}\rho)$, to get

$$\Psi(\rho, z, t) = e^{-i\omega_0 t} e^{iQz} \sum_{m=-N}^N A_m J_\mu(k_{\rho m}\rho) e^{i(2\pi/L)mz}. \quad (2.79)$$

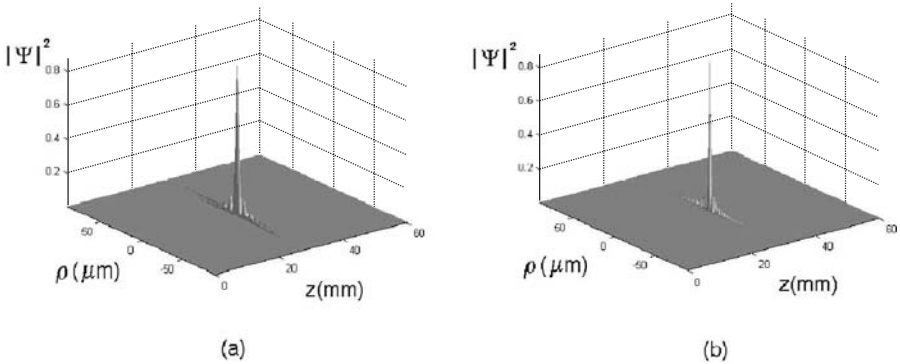


FIGURE 2.5 (a) Frozen wave with $Q = 0.999\omega_0/c$ and $N = 45$, approximately reproducing the longitudinal pattern chosen, represented by Eq. (2.77). (b) A different frozen wave, now with $Q = 0.995\omega_0/c$ (but still with $N = 45$), forwarding the same longitudinal pattern. We can observe that in this case (with a lower value for Q) a higher transverse localization is obtained.

With this, and based on intuitive arguments [17], we can expect that the longitudinal intensity pattern desired, constructed initially for $\rho = 0$, will shift approximately to $\rho = \rho'$, where ρ' represents the position of the first maximum of the Bessel function [i.e., the first positive root of the equation $(dJ_\mu(k_{\rho m=0} \rho)/d\rho)|_{\rho'} = 0$]. Using such a procedure, one can obtain very interesting stationary configurations of field intensity, as “donuts,” cylindrical surfaces, and much more.

In the following example, we show how to obtain, for example, a cylindrical surface of stationary light. To get it within the interval $0 \leq z \leq L$, let us first select the longitudinal intensity pattern given by Eq. (2.77), with $l_1 = L/2 - \Delta z$ and $l_2 = L/2 + \Delta z$, and with $\Delta z = L/300$. Moreover, let us choose $L = 0.05$ m, $Q = 0.998 \omega_0/c$, and use $N = 150$.

Then, after calculating the coefficients A_m by Eq. (2.73), we have recourse to superposition (2.79). In this case we choose $\mu = 4$. According to the previous discussion, one can expect the desired longitudinal intensity pattern to appear shifted to $\rho' \approx 5.318/k_{\rho m=0} = 8.47 \mu\text{m}$, where 5.318 is the value of $k_{\rho m=0} \rho$ for which the Bessel function $J_4(k_{\rho m=0} \rho)$ assumes its maximum value, with $k_{\rho m=0} = \sqrt{\omega_0^2 - Q^2}$. Figure 2.6 shows the resulting intensity field. In Fig. 2.6a the transverse section of the resulting beam for $z = L/2$ is shown. The transverse peak intensity is located at $\rho = 7.75 \mu\text{m}$, with a 8.5% difference with respect to the predicted value of $8.47 \mu\text{m}$. Figure 2.6b shows the orthogonal projection of the resulting field, which corresponds to a cylindrical surface of stationary light (or other fields).

We can see that the desired longitudinal intensity pattern has been obtained approximately, but, as desired, shifted from $\rho = 0$ to $\rho = 7.75 \mu\text{m}$, with the resulting field resembling a cylindrical surface of stationary light with radius $7.75 \mu\text{m}$ and length $238 \mu\text{m}$. Donut-like configurations of light (or sound) are also possible.

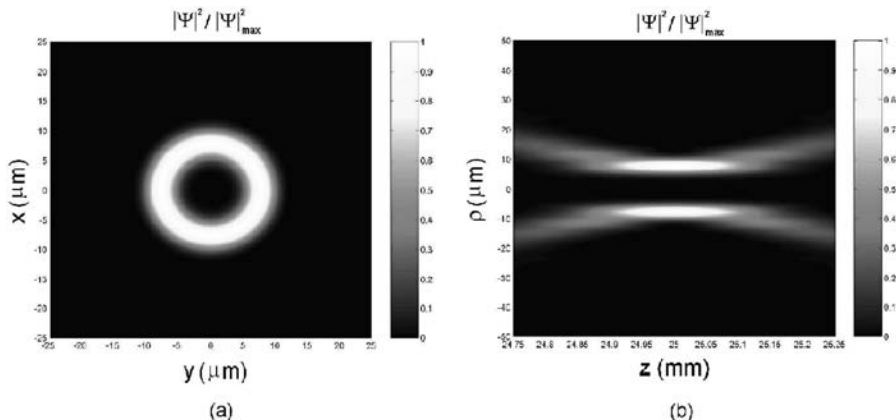


FIGURE 2.6 (a) Transverse section at $z = L/2$ of the higher-order FW. (b) Orthogonal projection of the three-dimensional intensity pattern of the same higher-order FW.

2.5.2 Stationary Wave Fields with Arbitrary Longitudinal Shape in Absorbing Media: Extending the Method

When propagating in a nonabsorbing medium, nondiffracting waves maintain their spatial shape for long distances. However, the situation is not the same when dealing with absorbing media. In this case, both ordinary and nondiffracting beams (and pulses) will suffer the same effect: an exponential attenuation along the propagation axis.

Here, we are going to extend [10] the method given above to show that through suitable superposition of equal-frequency Bessel beams, it is possible to obtain nondiffracting beams, in *absorbing media*, whose longitudinal intensity pattern can assume any shape desired within a chosen interval $0 \leq z \leq L$ of the propagation axis z . As a particular example, we obtain new nondiffracting beams capable of resisting the loss effects, maintaining the amplitude and spot size of their central core for long distances.

It is important to stress that this new method involves no active participation from the material medium. Actually, the energy absorption by the medium continues to occur normally, the difference being that these new beams have an initial transverse field distribution such that even in the presence of absorption, their central cores can be reconstructed for distances considerably longer than the penetration depths of ordinary (nondiffracting or diffracting) beams. In this sense, the present method can be regarded as extending, for absorbing media, the self-reconstruction properties [27] that normal localized waves are known to possess in lossless media.

In the same way as for lossless media, we construct a Bessel beam with angular frequency ω and axicon angle θ in the absorbing materials by superposing plane waves that have the same angular frequency ω and whose wave vectors lie on the surface of a cone with vertex angle θ . The refractive index of the medium can be written as

$n(\omega) = n_R(\omega) + in_I(\omega)$, the quantity n_R being the real part of the complex refraction index and n_I the imaginary part responsible for the absorbing effects. With a plane wave, the penetration depth δ for the frequency ω is given by $\delta = 1/\alpha = c/2\omega n_I$, where α is the absorption coefficient.

In this way, a zero-order Bessel beam in dissipative media can be written as $\psi = J_0(k_\rho \rho) \exp(i\beta z) \exp(-i\omega t)$ with $\beta = n(\omega)\omega \cos \theta/c = n_R\omega \cos \theta/c + in_I\omega \cos \theta/c \equiv \beta_R + i\beta_I$ and $k_\rho = n_R\omega \sin \theta/c + in_I\omega \sin \theta/c \equiv k_{\rho R} + ik_{\rho I}$, so $k_\rho^2 = n^2\omega^2/c^2 - \beta^2$. In this way, $\psi = J_0((k_{\rho R} + ik_{\rho I})\rho) \exp(i\beta_R z) \exp(-i\omega t) \exp(-\beta_I z)$, where β_R and $k_{\rho R}$ are the real parts of the longitudinal and transverse wavenumbers, and β_I and $k_{\rho I}$ are the imaginary parts. The absorption coefficient of a Bessel beam with an axicon angle θ is given by $\alpha_\theta = 2\beta_I = 2n_I\omega \cos \theta/c$, its penetration depth being $\delta_\theta = 1/\alpha_\theta = c/2\omega n_I \cos \theta$.

Due to the fact that k_ρ is complex, the amplitude of the Bessel function $J_0(k_\rho \rho)$ starts decreasing from $\rho = 0$ up to the transverse distance $\rho = 1/2k_{\rho I}$, and afterward it starts growing exponentially. This behavior is not physically acceptable, but one must remember that it occurs only because of the fact that an ideal Bessel beam requires an infinite aperture in order to be generated. However, in any real situation, when a Bessel beam is generated by finite apertures, that exponential growth in the transverse direction, starting after $\rho = 1/2k_{\rho I}$, will *not* occur indefinitely, stopping at a given value of ρ . Moreover, we emphasize that when generated by a finite aperture of radius R , the truncated Bessel beam [17] possesses a depth of field $Z = R/\tan \theta$ and can be described approximately by the solution given in the preceding paragraph for $\rho < R$ and $z < Z$.

Experimentally, to guarantee that exponential growth in the transverse direction does not even start, so as to generate only decreasing transverse intensity, the radius R of the aperture used to generate the Bessel beam should be $R \leq 1/2k_{\rho I}$. However, as noted by Durnin et al. [3], the same aperture also has to satisfy the relation $R \geq 2\pi/k_{\rho R}$. From these two conditions, we can infer that in an absorbing medium, a Bessel beam with decreasing transverse intensity can be generated only when the absorption coefficient is $\alpha < 2/\lambda$ (i.e., if the penetration depth is $\delta > \lambda/2$). The method developed in this subsection does refer to these cases; that is, we can always choose a suitable finite aperture size such that the truncated versions of all solutions presented here, including the general solution given by Eq. (2.80), will present no nonphysical behavior. Let us now present our method.

Consider an absorbing medium with the complex refraction index $n(\omega) = n_R(\omega) + in_I(\omega)$ and the following superposition of $2N + 1$ Bessel beams with the same frequency ω :

$$\Psi(\rho, z, t) = \sum_{m=-N}^N A_m J_0((k_{\rho R_m} + ik_{\rho I_m})\rho) e^{i\beta_{R_m} z} e^{-i\omega t} e^{-\beta_{I_m} z}, \quad (2.80)$$

where m represents integer numbers, A_m constant (yet unknown) coefficients, and β_{R_m} and $k_{\rho R_m}$ (β_{I_m} and $k_{\rho I_m}$) the real parts (the imaginary parts) of the complex longitudinal

and transverse wave numbers of the m th Bessel beam in superposition (2.80), with the following relations being satisfied:

$$k_{\rho_m}^2 = n^2 \frac{\omega^2}{c^2} - \beta_m^2 \quad (2.81)$$

$$\frac{\beta_{R_m}}{\beta_{I_m}} = \frac{n_R}{n_I}, \quad (2.82)$$

where $\beta_m = \beta_{R_m} + i\beta_{I_m}$ and $k_{\rho_m} = k_{\rho_{R_m}} + ik_{\rho_{I_m}}$, with $k_{\rho_{R_m}}/k_{\rho_{I_m}} = n_R/n_I$. Our goal now is to find the values of the longitudinal wave numbers β_m and the coefficients A_m in order to reproduce approximately, inside the interval $0 \leq z \leq L$ (on the axis $\rho = 0$), a freely chosen longitudinal intensity pattern that we call $|F(z)|^2$.

The problem for the particular case of lossless media [16,17] (i.e., when $n_I = 0 \rightarrow \beta_{I_m} = 0$) was solved earlier. For those cases it was shown that the choice $\beta = Q + 2\pi m/L$, with $A_m = \int_0^L F(z) \exp(-i2\pi m z/L)/L dz$, can be used to provide approximately the desired longitudinal intensity pattern $|F(z)|^2$ on the propagation axis within the interval $0 \leq z \leq L$, and at same time to regulate the spot size of the resulting beam by means of the parameter Q , which can also be used to obtain large depths of field and to validate the linear polarization approximation to the electric field in a transverse electromagnetic wave (see details in [16,17]).

However, when dealing with absorbing media, the procedure just described does not work, due to the presence of the functions $\exp(-\beta_{I_m} z)$ in the superposition (2.80), since in this case that series does not become a Fourier series when $\rho = 0$. To attempt to overcome this limitation, let us write the real part of the longitudinal wave number, in superposition (2.80), as

$$\beta_{R_m} = Q + \frac{2\pi m}{L}, \quad (2.83)$$

with

$$0 \leq Q + \frac{2\pi m}{L} \leq n_R \frac{\omega}{c}. \quad (2.84)$$

This inequality guarantees only forward propagation, with no evanescent waves. The superposition (2.80) can now be written as

$$\Psi(\rho, z, t) = e^{-i\omega t} e^{iQz} \sum_{m=-N}^N A_m J_0((k_{\rho_{R_m}} + ik_{\rho_{I_m}})\rho) e^{i(2\pi m/L)z} e^{-\beta_{I_m} z}, \quad (2.85)$$

where, by using (2.82), we have $\beta_{I_m} = (Q + 2\pi m/L)n_I/n_R$, and $k_{\rho_m} = k_{\rho_{R_m}} + ik_{\rho_{I_m}}$ is given by (2.81). Obviously, the discrete superposition (2.85) could be written as a continuous superposition (i.e., as an integral over β_{R_m}) by taking $L \rightarrow \infty$, but we prefer the discrete sum due to the difficulty of obtaining closed-form solutions to the integral form.

Now, let us examine the imaginary part of longitudinal wave numbers. The minimum and maximum values among the β_{I_m} are $(\beta_I)_{\min} = (Q - 2\pi N/L)n_I/n_R$ and $(\beta_I)_{\max} = (Q + 2\pi N/L)n_I/n_R$, the central value being given by $\bar{\beta}_I \equiv (\beta_I)_{m=0} = Qn_I/n_R$. With this in mind, let us evaluate the ratio $\Delta = [(\beta_I)_{\max} - (\beta_I)_{\min}]/\bar{\beta}_I = 4\pi N/LQ$.

Thus, when $\Delta \ll 1$, there are no substantial differences among the various β_{I_m} , since $\beta_{I_m} \approx \bar{\beta}_I$ holds for all m . In the same way, there are no substantial differences among the exponential attenuation factors, since $\exp(-\beta_{I_m}z) \approx \exp(-\bar{\beta}_I z)$. So when $\rho = 0$, the series in the right-hand side of Eq. (2.85) can be approximately considered a truncated Fourier series multiplied by the function $\exp(-\bar{\beta}_I z)$ and therefore superposition (2.85) can be used to reproduce approximately the desired longitudinal intensity pattern $|F(z)|^2$ (on $\rho = 0$), within $0 \leq z \leq L$, when the coefficients A_m are given by

$$A_m = \frac{1}{L} \int_0^L F(z) e^{\bar{\beta}_I z} e^{-i(2\pi m/L)z} dz, \quad (2.86)$$

the presence of the factor $\exp(\bar{\beta}_I z)$ in the integrand being necessary to compensate for the factors $\exp(-\beta_{I_m}z)$ in superposition (2.85). Since we are adding together zero-order Bessel functions, we can expect a good field concentration around $\rho = 0$.

In short, we have shown in this section how, in an absorbing medium, one can get a stationary wave-field with a good transverse concentration, whose longitudinal intensity pattern (on $\rho = 0$) can assume approximately any desired shape $|F(z)|^2$ within the predetermined interval $0 \leq z \leq L$. The method is a generalization of a previous method [16,17] and consists in the superposition of Bessel beams in (2.85), the real and imaginary parts of their longitudinal wave numbers being given by Eqs. (2.83) and (2.82) while their complex transverse wave numbers are given by Eq. (2.81) and the coefficients of the superposition are given by Eq. (2.86). The method is justified, since $4\pi N/LQ \ll 1$; happily enough, this condition is satisfied in many situations.

Regarding the generation of these new beams, given apparatus capable of generating a single Bessel beam, we can use an array of such apparatus to generate a group of beams with the appropriate longitudinal wave numbers and amplitudes/phases (as required by the method), thus producing the desired beam. For instance, we can use [16,17] a laser to illuminate an array of concentric annular apertures (located at the focus of a convergent lens), with the appropriate radii and transfer functions, able to yield both the correct longitudinal wave numbers (once a value for Q has been chosen) and the coefficients A_n of the fundamental superposition (2.85).

Some Examples For generality's sake, let us consider a hypothetical medium in which a typical XeCl excimer laser ($\lambda = 308 \text{ nm} \rightarrow \omega = 6.12 \times 10^{15} \text{ Hz}$) has a penetration depth of 5 cm (i.e., an absorption coefficient $\alpha = 20 \text{ m}^{-1}$, and therefore $n_I = 0.49 \times 10^{-6}$). Also let us suppose that the real part of the refractive index for this wavelength is $n_R = 1.5$ and therefore that $n = n_R + in_I = 1.5 + i 0.49 \times 10^{-6}$.

Note that the value of the real part of the refractive index is not very important since we are dealing with monochromatic wave fields.

A Bessel beam with $\omega = 6.12 \times 10^{15}$ Hz and an axicon angle $\theta = 0.0141$ rad (thus with a transverse spot of radius $8.4 \mu\text{m}$), when generated by an aperture, say, of radius $R = 3.5$ mm, can propagate in vacuum a distance (its depth of field) equal to $Z = R / \tan \theta = 25$ cm while resisting diffraction effects. However, in the material medium considered here, the penetration depth of this Bessel beam would be only $z_p = 5$ cm. Next, we give two interesting applications of this method.

Example 1 *Almost Undistorted Beams in Absorbing Media* We can use the extended method to obtain, in the same medium and for the same wavelength, an almost undistorted beam capable of preserving its spot size and the intensity of its central core for a distance many times larger than the typical penetration depth of an ordinary beam (nondiffracting or not). Let us suppose that for this material medium, we wish to have a beam (with $\omega = 6.12 \times 10^{15}$ Hz) that maintains the amplitude and spot size of its central core for a distance of 25 cm (i.e., a distance five times greater than the penetration depth of an ordinary beam of the same frequency). We can model this beam by choosing the desired longitudinal intensity pattern $|F(z)|^2$ (on $\rho = 0$) within $0 \leq z \leq L$:

$$F(z) = \begin{cases} 1 & \text{for } 0 \leq z \leq Z \\ 0 & \text{elsewhere} \end{cases} \quad (2.87)$$

and by setting $Z = 25$ cm, with, for example, $L = 33$ cm. Now, Bessel beam superposition (2.85) can be used to reproduce this intensity pattern approximately. Let us choose $Q = 0.9999\omega/c$ for the β_{R_m} in (2.83), and $N = 20$ [note that according to inequality (2.84), N could assume a maximum value of 158]. Once we have chosen the values of Q , L , and N , the values of the complex longitudinal and transverse Bessel beams wave numbers happen to be defined by relations (2.83), (2.82), and (2.81). Eventually, we can use Eq. (2.86) and find the coefficients A_m of the fundamental superposition (2.85) that defines the resulting stationary wave field. Note that the condition $4\pi N/LQ \ll 1$ is perfectly satisfied in this case.

In Fig. 2.7a we see the three-dimensional field intensity of the resulting beam. One can see that the field possesses good transverse localization (with a spot size smaller than $10 \mu\text{m}$) and is capable of maintaining the spot size and intensity of its central core up to the desired distance (a better result could be reached by using a higher value of N). It is interesting to note that at this distance (25 cm), an ordinary beam would have its initial field-intensity attenuated 148 times.

As we have said before, energy absorption by the medium continues to occur normally; the difference is that these new beams have an initial transverse field distribution that is sufficiently sophisticated to be able to reconstruct (even in the presence of absorption) their central cores up to a certain distance. For a better view of this field intensity distribution and of the energy flux, Fig. 2.7b shows the resulting beam in an orthogonal projection and logarithmic scale. It is clear that the energy comes from the lateral regions in order to reconstruct the central core of the beam. On the plane $z = 0$,

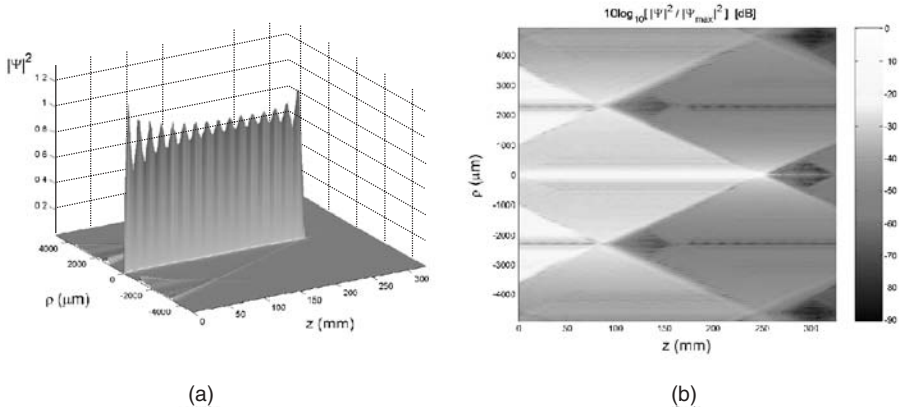


FIGURE 2.7 (a) Three-dimensional field intensity of the resulting beam. (b) The resulting beam, in an orthogonal projection and in logarithmic scale.

within the region $\rho \leq R = 3.5 \text{ mm}$, there is a uncommon field-intensity distribution, being very disperse instead of concentrated. This uncommon initial field-intensity distribution is responsible for constructing the central core of the resulting beam and for its reconstruction up to the distance $z = 25 \text{ cm}$. Due to the absorption, the beam (total) energy flowing through different z -planes is not constant, but the energy flowing through the beam spot area, and the beam spot size itself, are conserved up to (in this case) $z = 25 \text{ cm}$.

Example 2 Beams in Absorbing Media with a Growing Longitudinal Field Intensity. Again considering a hypothetical medium in which an ordinary Bessel beam with $\theta = 0.0141 \text{ rad}$ and $\omega = 6.12 \times 10^{15} \text{ Hz}$ has a penetration depth of 5 cm , we aim next to construct a beam that instead of possessing a constant core intensity up to $z = 25 \text{ cm}$ presents moderate exponential growth of its intensity up to that distance.

Let us assume that we wish to get a longitudinal intensity pattern $|F(z)|^2$ in the interval $0 < z < L$:

$$F(z) = \begin{cases} \exp(z/Z) & \text{for } 0 \leq z \leq Z \\ 0 & \text{elsewhere} \end{cases} \quad (2.88)$$

with $Z = 25 \text{ cm}$ and $L = 33 \text{ cm}$. Again using $Q = 0.9999\omega/c$, $N = 20$, we proceed as in example 1, calculating the complex longitudinal and transverse Bessel beams wave numbers and finally, the coefficients A_m of the fundamental superposition (2.85). In Fig. 2.8 we see the three-dimensional field intensity of the resulting beam. One can see that the field presents the desired longitudinal intensity pattern with good transverse localization (a spot size smaller than $10 \mu\text{m}$).

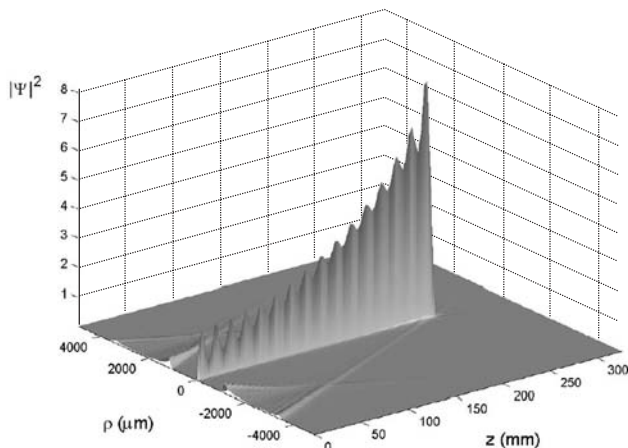


FIGURE 2.8 Three-dimensional field intensity of the resulting beam, in the absorbing medium, with a growing longitudinal field intensity.

Obviously, the amount of energy necessary to construct these new beams is greater than that necessary to generate an ordinary beam in a nonabsorbing medium. It is also clear that there is a limitation on the depth of field of these new beams. In example 1, for distances longer than 10 times the penetration depth of an ordinary beam, in addition to a greater energy demand, the field intensity in the lateral regions would be even higher than that of the core, and the field would lose the usual beam characteristics (i.e., transverse field concentration).

REFERENCES

1. A much more complete list of references may be found in Chapter 1.
2. J. N. Brittingham, Focus wave modes in homogeneous Maxwell's equations: transverse electric mode, *J. Appl. Phys.* **54**, 1179–1189 (1983).
3. J. Durmin, J. J. Miceli, and J. H. Eberly, Diffraction-free beams, *Phys. Rev. Lett.* **58**, 1499–1501 (1987).
4. J.-Y. Lu and J. F. Greenleaf, Nondiffracting X-waves: exact solutions to free-space wave equation and their finite aperture realizations, *IEEE Trans. Ultrason. Ferroelectr. Freq. Control* **39**, 19–31 (1992), and refs. therein.
5. H. Sõnajalg and P. Saari, Suppression of temporal spread of ultrashort pulses in dispersive media by Bessel beam generators, *Opt. Lett.* **21**, 1162–1164 (1996).
6. M. Zamboni-Rached, K. Z. Nóbrega, H. E. Hernández-Figueroa, and E. Recami, Localized superluminal solutions to the wave equation in (vacuum or) dispersive media, for arbitrary frequencies and with adjustable bandwidth, *Opt. Commun.* **226**, 15–23 (2003).
7. M. A. Porras, R. Borghi, and M. Santarsiero, Suppression of dispersion broadening of light pulses with Bessel–Gauss beams, *Opt Commun.* **206**, 235–241 (2003).

8. C. Conti, S. Trillo, P. Di Trapani, G. Valiulis, A. Piskarskas, O. Jedrkiewicz, and J. Trull, Nonlinear electromagnetic X-waves, *Phys. Rev. Lett.* **90**, 170406 (May 2003), and refs. therein.
9. J. Salo, J. Fagerholm, A. T. Friberg, and M. M. Salomaa, Nondiffracting bulk-acoustic X waves in crystals, *Phys. Rev. Lett.* **83**, 1171–1174 (1999), and refs. therein.
10. M. Zamboni-Rached, Diffraction–attenuation resistant beams in absorbing media, *Opt. Express* **14**, 1804–1809 (2006).
11. I. M. Besieris, A. M. Shaarawi, and R. W. Ziolkowski, A bidirectional traveling plane wave representation of exact solutions of the scalar wave equation, *J. Math. Phys.* **30**, 1254–1269 (1989).
12. M. Zamboni-Rached, Localized waves: structure and applications, M.Sc. thesis, Physics Department, Unicamp, São Paulo, Brazil, 1999.
13. M. Zamboni-Rached, E. Recami, and H. E. Hernández-Figueroa, New localized superluminal solutions to the wave equations—with finite total energies and arbitrary frequencies, *Euro. Phys. J. D* **21**, 217–228 (2002).
14. M. Zamboni-Rached, Localized waves in diffractive/dispersive media, Ph.D. dissertation, DMO/FEEC Universidade Estadual de Campinas, Campinas, Brazil, Aug. 2004; <http://libdigi.unicamp.br/document/?code=vtls000337794>.
15. S. Longhi, Localized subluminal envelope pulses in dispersive media, *Opt. Lett.* **29**, 147–149 (2004), and refs. therein.
16. M. Zamboni-Rached, Stationary optical wave fields with arbitrary longitudinal shape by superposing equal frequency Bessel beams: frozen waves, *Opt. Express* **12**, 4001–4006 (2004).
17. M. Zamboni-Rached, E. Recami, and H. E. Hernández-Figueroa, Theory of frozen waves: modelling the shape of stationary wave fields, *J. Opt. Soc. Am. A* **22**, 2465–2475.
18. S. V. Kukhlevsky and M. Mechler, Diffraction-free subwavelength-beam optics at nanometer scale, *Opt. Commun.* **231**, 35–43 (2004).
19. I. S. Gradshteyn and I. M. Ryzhik, *Integrals, Series and Products*, 4th ed., Academic Press, New York, 1965.
20. A. M. Shaarawi, I. M. Besieri, and T. M. Said, Temporal focusing by use of composite X-waves, *J. Opt. Soc. Am. A* **20**, 1658–1665, (Aug. 2003).
21. M. Zamboni-Rached, A. Shaarawi, and E. Recami, Focused X-shaped pulses, *J. Opt. Soc. Am. A* **21**, 1564–1574 (2004).
22. M. Zamboni-Rached, H. E. Hernández-Figueroa, and E. Recami, Chirped optical X-type pulses, *J. Opt. Soc. Am. A* **21**, 2455–2463 (2004).
23. G. Agrawal, *Nonlinear Fiber Optics*, 4th ed., Academic Press, San Diego, CA, 2006.
24. Z. Bouchal and M. Olivik, Non-diffractive vector Bessel beams, *J. Mod. Opt.* **42**, 1555–1566 (1995).
25. E. Recami, On localized X-shaped superluminal solutions to Maxwell equations, *Physica A*, **252**, 586–610 (1998).
26. Z. Bouchal, Controlled spatial shaping of nondiffracting patterns and arrays, *Opt. Lett.* **27**, 1376–1378 (2002).
27. R. Grunwald, U. Griebner, U. Neumann, and V. Kebbel, Self-reconstruction of ultrashort-pulse Bessel-like X-waves, presented at CLEO/QELS 2004, San Francisco, CA, May 16–21, 2004, *Conference Digest* (CD-ROM), paper CMQ7.